Marine and Petroleum Geology 120 (2020) 104527

Contents lists available at ScienceDirect

Marine and Petroleum Geology

journal homepage: www.elsevier.com/locate/marpetgeo

Research paper

Characteristics of molecular nitrogen generation from overmature black shales in South China: Preliminary implications from pyrolysis experiments

Haifeng Gai[a], Hui Tian[a,*], Peng Cheng[a], Chunmin He[a,b], Zijin Wu[a,b], Sui Ji[a], Xianming Xiao[c]

[a] State Key Laboratory of Organic Geochemistry, Guangzhou Institute of Geochemistry, Chinese Academy of Sciences, Guangzhou, 510640, China
[b] University of Chinese Academy of Sciences, Beijing, 100049, China
[c] School of Energy Resources, China University of Geosciences, Beijing, 100083, China

ARTICLE INFO

Keywords:
Shale gas
Molecular nitrogen
Thermal maturity
Sichuan Basin

ABSTRACT

High content of molecular nitrogen (N_2) is one of the natural gas exploration risks in petroliferous basins where black shales act as source rocks of either hydrocarbon gas or molecular nitrogen. In this study, two overmature and one low-maturity shale samples and their kerogens were investigated to determine the generation characteristics of molecular nitrogen as well as methane and the differences in the release processes of inorganic nitrogen fixed in ammonium-bearing minerals and organic nitrogen bound in kerogen. The results illustrate that with increasing pyrolysis temperature, the yield of methane first increases and then decreases with an inflection temperature of 650 °C (EqVRo = 3.4%), whereas the yield of molecular nitrogen shows a continuous increase throughout the pyrolysis experiment. The molecular nitrogen during the stage of methane generation (i.e., EqVRo < 3.4%) is more preferentially derived from the inorganic nitrogen in ammonium-bearing minerals, whereas the significant generation of molecular nitrogen from organic nitrogen in kerogen commences only after the methane generation potential is exhausted (EqVRo > 3.4%). The results also reveal that at the experimental maxima of thermal maturity (EqVRo = 4.9%), the generation potential of inorganic molecular nitrogen (mg/g N_{inorg}) is much lower than that of organic molecular nitrogen (mg/g N_{org}), indicating that in our experiments the organic nitrogen in kerogen is more easily to be converted into molecular nitrogen than the inorganic nitrogen in ammonium-bearing minerals. All these results indicate that molecular nitrogen content in shale gas may change dramatically during thermal evolution, and source rocks with exceptionally high maturity and high abundance of organic nitrogen likely lead to a high molecular nitrogen risk, particularly in regions of poor preservation conditions of shale gas, which may be the main reasons for the high molecular nitrogen content in the Lower Cambrian shale gas in South China.

1. Introduction

During past decades, various studies have investigated the geological carbon and nitrogen cycle from the atmosphere to deep strata (Falkowski, 1997; Kump and Arthur, 1999; Marty and Dauphas, 2003; Deutsch et al., 2007; Lam et al., 2009; Canfield et al., 2010; Maloof et al., 2010; Busigny et al., 2013; Stüeken et al., 2016; Wang et al., 2018; Mettam et al., 2019). Sedimentary rocks are an important carbon and nitrogen pool (Brandes et al., 2007; Algeo et al., 2008; Stüeken et al., 2016; Wang et al., 2015, 2018), and the carbon and nitrogen elements are derived from both organic and inorganic contributions (Boyd, 2001; Leithold et al., 2016; Stüeken et al., 2017). The mineralization of C and N during early diagenesis is controlled by the nature of biomass, microbial activity, oxygen availability, temperature/thermal stress, sedimentation rate, and fluid-rock interactions; thus, the contents of carbon and nitrogen in sediments may be highly variable (Boyd, 2001; Jurisch et al., 2012; Leithold et al., 2016; Stüeken et al., 2017). Thermal and chemical degradation processes lead to the loss of carbon and nitrogen in sedimentary rocks as diagenesis and catagenesis proceed (Behar et al., 2000; Kelemen et al., 1998, 2006; Boudou et al., 2008; Jurisch et al., 2012). One of the main ways to release carbon and nitrogen from sedimentary rocks is by the formation of gases, which is also one of the important processes in carbon and nitrogen cycle (Falkowski, 1997; Deutsch et al., 2007; Canfield et al., 2010; Stüeken et al., 2016; Wang et al., 2018).

Molecular nitrogen is one of the most common non-hydrocarbons in natural gas (Jenden et al., 1988; Dai, 1992; Littke et al., 1995; Zhu et al., 2000; Kotarba and Nagao, 2008, 2014; Liu et al., 2012). Although most conventional natural gases contain only a few percent of molecular nitrogen (N_2), N_2-rich natural gas in reservoir rocks is also known

* Corresponding author. 511 Kehua Road, Tianhe District, Guangzhou City, Guangdong Province, China.
E-mail address: tianhui@gig.ac.cn (H. Tian).

https://doi.org/10.1016/j.marpetgeo.2020.104527
Received 2 January 2020; Received in revised form 7 June 2020; Accepted 8 June 2020
Available online 12 June 2020

in many basins around the world (Krooss et al., 1995; Littke et al., 1995; Zhu et al., 2000; Chen and Zhu, 2003; Dai et al., 2005; Mingram et al., 2005; Liu et al., 2012). Previous studies have suggested several possible origins of molecular nitrogen in natural gas, including decomposition of sedimentary organic matter and/or minerals, primordial nitrogen from deep mantle, and radiogenic, atmospheric and magmatic processes (e.g. Maksimov, 1975; Allègre et al., 1987; Gold and Held, 1987; Andersen et al., 1993; Baxby et al., 1994; Krooss et al., 1995, 2005; Zhu et al., 2000; Dai et al., 2005; Mingram et al., 2005; Liu et al., 2012; Kotarba et al., 2014). Among the above sources, thermal degradation is one of the most common process for N_2 accumulation in natural gas pools, which has been experimentally confirmed by many authors (Boudou and Espitalié, 1995, 2008; Krooss et al., 1995; Littke et al., 1995; Behar et al., 2000; Kelemen et al., 2006; Heim et al., 2012; Jurisch and Krooss, 2008, 2012). In addition, some post-genetic processes may also lead to the relative enrichment of molecular nitrogen in natural gas. They include the thermochemcial sulfate reduction (TSR) reactions (Liu et al., 2012; Jenden et al., 2015), the loss of early generated methane due to tectonic activity (Su et al., 2019; Wu et al., 2019), and the competitive adsorption/desorption between molecular nitrogen via reducing the partial pressure of methane in shales or coals (Bustin et al., 2016; Zhang et al., 2017; Li and Elsworth, 2019; Ghalandari et al., 2020).

Molecular nitrogen, though worthless from a commercial point of view, is probably a key to an improved understanding of the formation mechanisms, longevity and compositional evolution of natural gas accumulations on the geologic time scale, and therefore is a valuable study object for geoscientists (Krooss et al., 1995; 2005; Mingram et al., 2005; Kotarba et al., 2014). Moreover, high molecular nitrogen content reduces the methane concentration in natural gas and is bound to pose a serious risk in natural gas exploration (Littke et al., 1995). Recently, a high content of molecular nitrogen has been encountered in some overmature Lower Cambrian shale gas in southeastern Chongqing and northern Guizhou, China (Liu et al., 2016); Jiao et al. (2017b). Liu et al., 2016 reported that these high contents of molecular nitrogen is mainly of thermal origin in terms of their nitrogen isotopic composition. However, the Lower Silurian shales, another set of overmature Lower Paleozoic shale strata in the same area, has not exhibited a high content of molecular nitrogen (Dai et al., 2014). Therefore, the mechanism, timing, and potential of molecular nitrogen generation in Lower Paleozoic shale gas in the Upper Yangtze region still requires further investigation.

In this study, one Lower Cambrian shale sample and one Lower Silurian shale sample that display similar thermal maturity, organic matter abundance, and kerogen type but different nitrogen content and species were selected from two wells in the Upper Yangtze region to investigate their release characteristics of organic nitrogen in kerogen and inorganic nitrogen in ammonium-bearing minerals. In addition, nitrogen release from a low-maturity shale sample from the Mesoproterozoic was also studied for comparison with the two overmature Lower Paleozoic shales. This study may help to evaluate the molecular nitrogen generation potential of organic-rich shale during thermal maturation and to understand the risk of high content of molecular nitrogen in overmature shale gas.

2. Geological setting

The Sichuan Basin, which is located in the Yangtze platform, is one of the main natural gas province in China. Marine shales were widely developed during the early Paleozoic in Sichuan Basin and its peripheral areas, including the Lower Silurian to Upper Ordovician and the Lower Cambrian shales. The Lower Silurian Longmaxi Formation has become the most important marine shale gas-producing layer in China (Zou et al., 2010, 2015; Zeng et al., 2012; Tian et al., 2013; Dai et al., 2014) and consists of black shales and silty shales in its lower section where graptolite fossils are abundant (Liang et al., 2012). Kerogen types of the organic matter in the black shales of the Longmaxi Formation is dominated by types I and II, with equivalent vitrinite reflectance (EqVRo) values in the range of 2.0–3.5% (Zou et al., 2010; Tian et al., 2013; Dai et al., 2016; Pan et al., 2016). The total organic carbon (TOC) contents of the Longmaxi shales are lower in the southwestern areas of the Sichuan Basin, ranging from 0.5 to 1.0%, but become higher in the eastern part of the basin, ranging from 1.0 to 4.0% (Tian et al., 2013).

Black shale formed during early Cambrian in the Upper Yangtze region is named the Niutitang Formation or the Jiumenchong Formation in Guizhou Province, the Qiongzhusi Formation in the Sichuan Basin, and the Shuijingtuo Formation in northeastern Chongqing (Zeng et al., 2012; Tian et al., 2015; Liu et al., 2016b; Li et al., 2017). The Lower Cambrian shales are more organic-rich but display higher thermal maturity levels than the Lower Silurian shales, having EqVRo values mostly greater than 3.0% (Nie et al., 2011; Hao et al., 2013; Tan et al., 2014; Tian et al., 2015; Li et al., 2017). Lower Cambrian shales are considered to have good shale gas potential due to their wide distribution, large thickness, and high TOC content (e.g., Zou et al., 2010, 2015; Tan et al., 2013; Tian et al., 2013, 2015; Dai et al., 2014; Liu et al., 2016b; Li et al., 2017). However, only few industrial shale gas plays have been discovered in the Lower Cambrian shales in Sichuan Basin and its surrounding areas. Furthermore, the Lower Cambrian shale gas is often rich in molecular nitrogen, leading to a very low content of hydrocarbon gases such as methane (Liu et al., 2016b; Jiao et al., 2017).

3. Samples and methods

3.1. Samples

Sixteen core samples of Lower Silurian Longmaxi shale and sixteen Low Cambrian Shuijingtuo shale were collected from wells YC4 and YC2 in southeastern and northeastern Chongqing, respectively (Fig. 1; Table 1). Based on the quantity of core samples and their geochemical characteristics, one typical Longmaxi shale sample at the depth of 745.8 m of Well YC4 and one Low Cambrian Shuijingtuo shale sample at the depth of 1101.9 m of YC2 were selected for pyrolysis experiments and named YC4R and YC2R, respectively (Table 1).

For a comparative purpose, a low-maturity black shale sample, named J7R, was also collected from the outcrop of the Mesoproterozoic Xiamaling Formation in Hebei Province, China. In addition, a vitrinite-rich coal sample with a vitrinite reflectance (VRo) value of 0.56% was also pyrolyzed under the same conditions as the shales to determine the VRo values at different pyrolysis temperatures.

3.2. Organic geochemistry, minerology, and nitrogen structure characteristics

The three selected raw shale samples YC2R, YC4R, and J7R were first crushed into powders (100 mesh) and then treated with hydrochloric and hydrofluoric acids (HCl and HF) to obtain the kerogen samples YC2K, YC4K, and J7K, respectively.

The TOC contents of the shale samples were measured with a Leco CS230 Carbon/Sulfur analyzer after carbonate removal by diluted hydrochloric acid treatment, and the TOC values of kerogen samples was measured directly with the same instruments as for shale samples.

Elemental nitrogen contents of shales and kerogens were performed using a Vario EL III instrument (Elementar Analysensysteme GmbH). The temperatures of the oxidation oven and reduction furnace were 950 °C and 600 °C, respectively. Acetanilide and a standard sediment sample (AEB 2151) were used to calibrate the measurement results. Measurements were repeated at least three times for each sample and the relative error is smaller than 5%.

Pyrobitumen reflectances of the three raw shale samples and vitrinite reflectances of the vitrinite-rich original and pyrolyzed coal samples at different pyrolysis temperatures were measured using a 3Y-Leica DMR XP microscopy equipped with a microphotometer. The

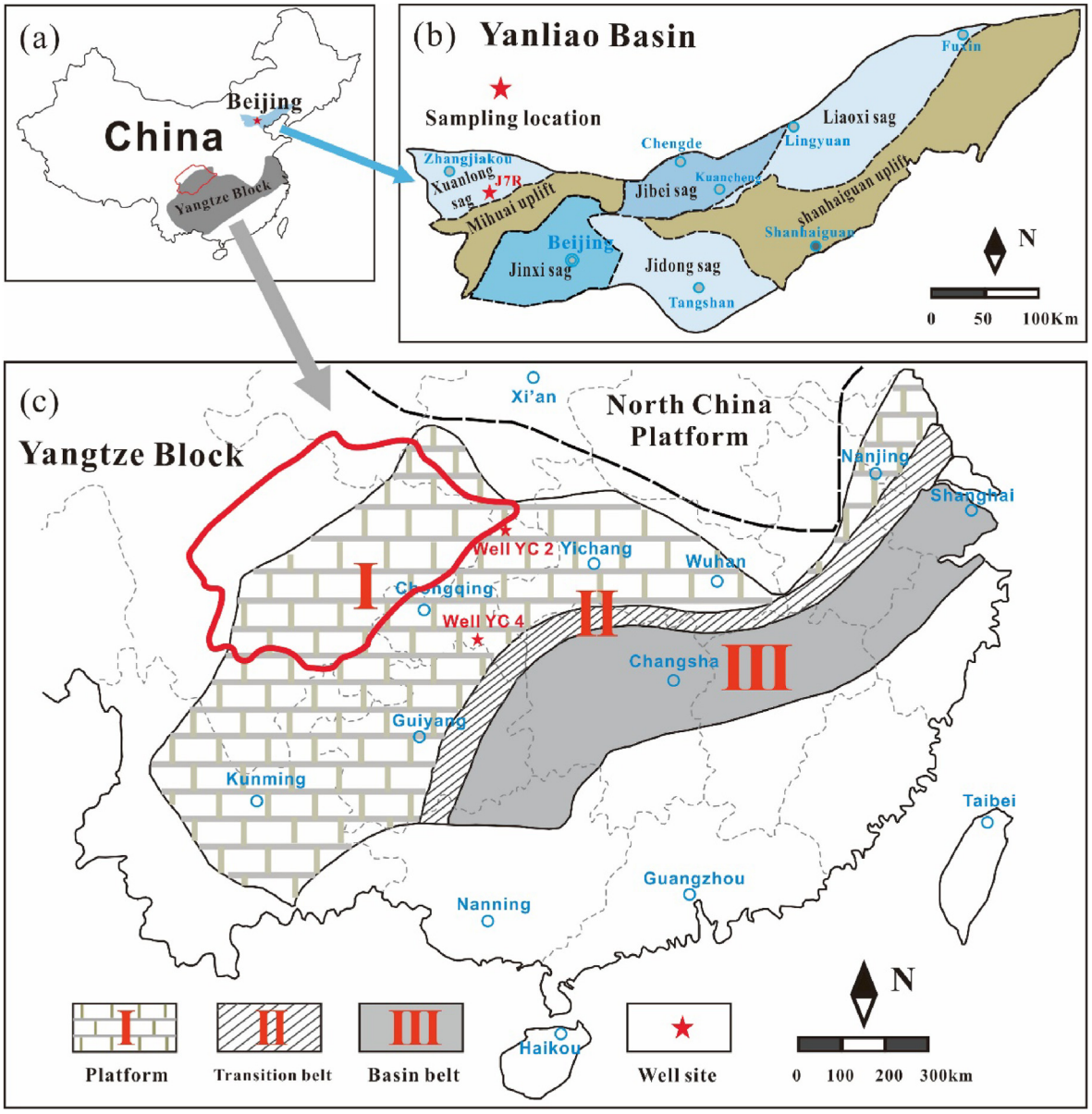

Fig. 1. Schematic maps showing the sampling locations. (a) Geographical location of the Yangtze Platform and the Yanliao Basin; (b) The tectonic subdivisions of the Yanshan Basin and the sampling location of Xiamaling shale (modified from Luo et al., 2016); (c) Simplified geological map of the Yangtze Platform (modified from Yin et al., 2018), and the location of well YC2 and well YC4 in Chongqing.

random reflectance was measured in oil immersion (n = 1.518) at 546 nm using a 50 × /0.85 objective lens and the reported values were determined by averaging 50 measurements on pyrobitumen or vitrinite particles.

X-ray diffraction (XRD) analysis of shale powders was carried out on a Bruker D8 Advance X-ray diffractometer at 40 kV and 30 mA with Cu Ka radiation (λ = 1.5406 for CuKα1). Stepwise scanning measurements were performed at a rate of 4°/min in the range of 3–85° (2θ). The relative contents of main minerals were estimated semi-quantitatively based on the areas of their major peaks with Lorentz polarization correction (Pecharsky and Zavalij, 2003).

Nondestructive X-ray photoelectron spectroscopy (XPS), which offers an approach to monitor maturity-related changes in the chemical character of nitrogen (Boudou et al., 2008), was performed on both shale and kerogen samples. The XPS analysis procedure has been well illustrated in Boudou et al. (2008) and Liu et al. (2016a). Briefly, powdered samples were pressure-mounted onto conducting indium foils. XPS measurements were performed using a K-Alpha X-ray photoelectron spectrometer (Thermo Fisher Scientific, UK) with a monochromatic Al K X-ray source (excitation energy = 1468.6 eV). Spectra were collected from 0 to 1350 eV using an X-ray spot size of 400 μm with a pass energy of 100 eV for wide scans and 30 eV for individual elements. Binding energies were corrected relative to the carbon 1s signal at 284.8 eV. Binding energy values were determined with a precision of ± 0.1 eV. The XPS data analysis was completed using Avantage software (Thermo Scientific™, version 5.934). After deducting the background contribution, the N 1s spectra were curve-fitted with the minimum number of mixed Gaussian–Lorentzian component profiles. Chemical–structural assignments of N 1s XPS subpeaks including N-6, N-5, N-Q1, N-Q2, and N-X were first guided by known binding energies of nitrogen in model compounds and purified substrates (NIST XPS database, Boudou et al., 2008), and then their peak intensity and peak position were further optimized with Avantage software to best fit the measured N 1s XPS spectra (Liu et al., 2016a).

Table 1
TOC and total nitrogen contents of the shale samples collected from well YC2 and well YC4.

Well	Depth	Formation	Lithology	TOC (wt.%)	N_{tot}[a] (mg/g)	Well	Depth	Formation	Lithology	TOC (wt.%)	N_{tot} (mg/g)
YC2	941.4	Shuijingtuo Formation	Black shale	2.89	2.46	YC4	645.5	Longmaxi Formation	Black shale	1.35	1.35
YC2	956.6	Shuijingtuo Formation	Black shale	2.94	2.17	YC4	649.7	Longmaxi Formation	Black shale	1.45	1.44
YC2	1004.2	Shuijingtuo Formation	Black shale	2.53	1.91	YC4	652.5	Longmaxi Formation	Black shale	1.35	1.45
YC2	1014.2	Shuijingtuo Formation	Black shale	1.84	1.57	YC4	659.6	Longmaxi Formation	Black shale	3.15	1.17
YC2	1023.9	Shuijingtuo Formation	Black shale	1.80	2.15	YC4	665.7	Longmaxi Formation	Black shale	1.59	1.53
YC2	1047.7	Shuijingtuo Formation	Black shale	2.37	1.89	YC4	676.6	Longmaxi Formation	Black shale	2.19	1.55
YC2	1055.8	Shuijingtuo Formation	Black shale	2.39	1.66	YC4	683.5	Longmaxi Formation	Black shale	2.82	1.87
YC2	1078.9	Shuijingtuo Formation	Black shale	3.79	2.81	YC4	690.0	Longmaxi Formation	Black shale	1.17	1.27
YC2	1086.9	Shuijingtuo Formation	Black shale	2.54	1.63	YC4	698.4	Longmaxi Formation	Black shale	1.78	1.48
YC2	1091.2	Shuijingtuo Formation	Black shale	2.31	1.71	YC4	709.5	Longmaxi Formation	Black shale	1.62	1.47
[b]YC2	**1101.9**	**Shuijingtuo Formation**	**Black shale**	**3.19**	**2.51**	YC4	717.6	Longmaxi Formation	Black shale	1.37	1.44
YC2	1109.7	Shuijingtuo Formation	Black shale	2.07	1.67	YC4	727.8	Longmaxi Formation	Black shale	2.57	1.59
YC2	1115.7	Shuijingtuo Formation	Black shale	1.69	1.63	**[b]YC4**	**745.8**	**Longmaxi Formation**	**Black shale**	**3.35**	**1.55**
YC2	1130.9	Shuijingtuo Formation	Black shale	2.40	2.02	YC4	755.6	Longmaxi Formation	Black shale	4.33	1.37
YC2	1134.4	Shuijingtuo Formation	Black shale	2.57	2.17	YC4	757.4	Longmaxi Formation	Black shale	3.69	0.97
YC2	1147.7	Shuijingtuo Formation	Black shale	1.38	1.58	YC4	761.3	Longmaxi Formation	Black shale	4.51	1.74

[a] N_{tot}: total nitrogen content of shale sample.
[b] Shale samples used for pyrolysis experiments.

3.3. Pyrolysis experiment and product analysis

Anhydrous pyrolysis experiments on the three selected shale samples and their corresponding kerogen samples were carried out under vacuum in a programmed muffle furnace. Procedures of such kind of experimental have been described in Chen and Xiao (2014). Briefly, a certain amount of shale samples (0.5–5.0 g) or kerogen samples (0.2–1.0 g), which were pre-dried for 24 h at 60 °C in a vacuum oven, were loaded into a series of quartz tubes (with an inner diameter of 30 mm and a volume of 100.9 mL). Each tube was evacuated for 5 min to displace the residual air in the tube and then sealed with oxyhydrogen flame (Fig. 2a).

The three shale samples, three kerogen samples and vitrinite-rich coal were simultaneously heated in the furnace from room temperature to a preset temperature at a heating rate of 200 °C/h and then hold for 24 h. The pyrolysis temperatures of overmature shale samples YC2R and YC4R and their kerogen counterparts were set within the range 600–900 °C with 25 or 50 °C intervals, whereas those for the low-maturity shale sample J7R and its kerogen counterpart, along with the vitrinite-rich coal samples, were set within the range of 300–900 °C. Once the designed pyrolysis temperature and time were reached, the furnace was opened, and the quartz tubes were removed after their temperatures dropped below 100 °C. Every heating run was performed on a new batch of powdered samples. During experiments, the accuracy of temperature measurements was better than ± 0.5 °C.

The yields of methane and molecular nitrogen generated from shales and kerogens were measured with an Agilent 7890 A gas chromatography (GC). The gas collecting device and analytical procedure are similar to those adopted by Pan et al. (2006) and shown in Fig. 2b. When valve A is opened and valves B, C, and D are shut down, the whole device was evacuated to an internal pressure of less than 1×10^{-2} Pa. After the entire device was evacuated, a thin top of the tube was crushed by a plier to release the pyrolytic gas into the vacuumed system (Fig. 2b). After 60 s, gas components fill the whole system except the segment between valves B and C. When valve B is opened, a specific amount of gas was automatically introduced into the GC system.

The GC is equipped with one flame ionization detector (FID) and two thermal conductivity detector (TCD) for analyzing gas hydrocarbons and nonhydrocarbons, and high-purity helium (99.9999%) was used as carrier gas. The oven temperature for gas analysis was initially held at 70 °C for 6 min, ramped from 70 to 180 °C at 15 °C/min, and then held at 180 °C for 4 min. A test with external standard gases indicated that this device has a relative error of less than 0.5% for methane and of less than 4.0% for molecular nitrogen.

After the gas components were analyzed, the solid residues at each temperature point were recovered and subjected to analyses of TOC content, nitrogen content and XPS.

4. Results and discussion

4.1. Organic geochemistry and mineralogy

In general, Longmaxi shales collected from well YC4 had a TOC range of 1.2–4.5% with total nitrogen content (N_{tot}) ranging from 1.0 to 1.9 mg/g shale, whereas the range of TOC and N_{tot} contents of Lower

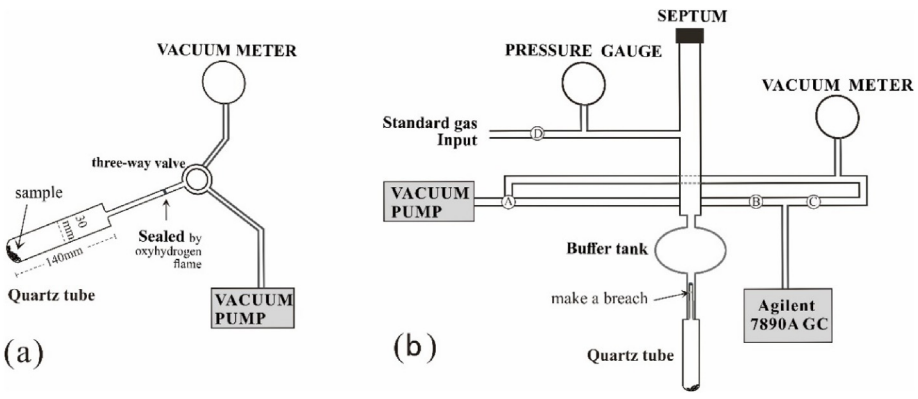

Fig. 2. Schematic diagram showing the quartz tube pyrolysis system for sealing quartz tubes (a) and gas analysis (b, modified from Pan et al., 2006).

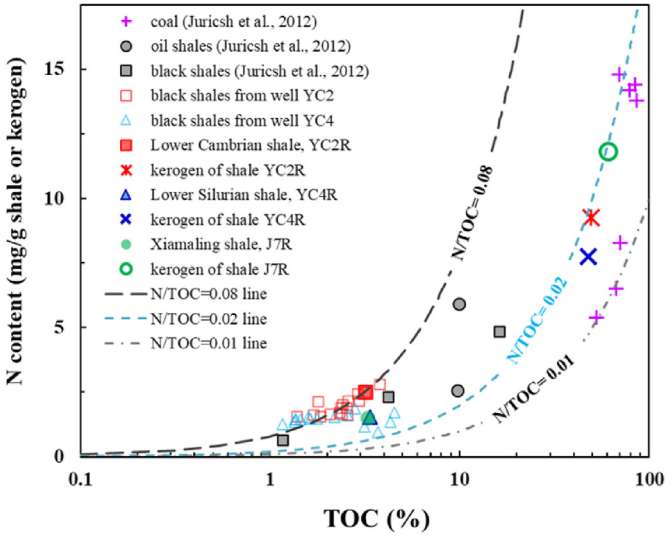

Fig. 3. Nitrogen content versus total organic carbon (TOC) content for the three shales and their kerogen samples. The N/TOC ratios for coal or kerogen samples are mainly between 0.01 and 0.02, and N/TOC ratios greater than 0.02 indicate the presence of inorganic nitrogen.

Cambrian shales collected from well YC2 are 1.4–3.8% and 1.6–2.8 mg/g shale, respectively (Table 1; Fig. 3). The black shales from the two wells have similar TOC contents but distinct N_{tot} contents, which is beneficial to their comparative study of nitrogen release during pyrolysis.

The two selected shales for pyrolysis experiments, i.e., the Lower Cambrian shale sample YC2R and the Lower Silurian shale sample YC4R, have respective TOC contents of 3.19% and 3.35% (Table 2). The organic fraction of the Lower Paleozoic shales in the study area is dominated by maceral assemblages of micrinite and pyrobitumen formed by the cracking of retained oil in shales (Tian et al., 2013, 2015). The measured mean pyrobitumen reflectance values for samples YC2R and YC4R are 2.85% and 3.04% (Table 2), respectively, indicating that they have similar maturity levels and both are within the stage of dry gas generation. The Mesoproterozoic Xiamaling sample J7R has a TOC content of 3.26%, whose organic fraction is dominated by bitumen, lamalginite, liptodetrinite, and amorphous organic matter (AOM) (Zhang et al., 2007). This sample has a measured mean bitumen reflectance of 0.74%, and the Tmax value from Rock-Eval pyrolysis is 437 °C, which corresponds to an EqVRo value of 0.71% based on the equation of EqVRo = 0.018 × Tmax −7.16 (Jarvie et al., 2001), indicating an early mature stage with respective to hydrocarbon generation (Table 2).

The mineralogical compositions of samples YC2R and YC4R are dominated by quartz and clays (greater than 70%), and these two shales have similar amounts of feldspar and pyrite but the former has lower quartz content (27.4%) and higher carbonate content (14.6%) than the latter (40.9% and 5.5%, respectively). Sample J7R is also dominated by quartz (51.8%) and clays (36.3%), and has a feldspar content and a carbonate content of 9.3% and 2.6%, respectively.

Table 2 presents the nitrogen contents of the three shales and their kerogens. Although the TOC contents of the three shale samples are similar, their N_{tot} are quite different. Sample YC2R has a N_{tot} value of 2.51 mg/g shale and a N_{tot}/TOC ratio of 0.0787; samples YC4R and J7R have similar N_{tot} values (1.52–1.55 mg/g shale) and N_{tot}/TOC ratios (0.0463–0.0466) (Table 2). The kerogen nitrogen (organic nitrogen, N_{org}) contents range from 7.76 to 11.84 mg/g kerogen; however, the kerogens have lower N_{org}/TOC_k ratios, which are in the range of 0.0162–0.0196, much lower than the shale samples (Table 2). Early studies have illustrated that the nitrogen contents of coals or kerogens (all the nitrogen is regarded as organic nitrogen) range mostly from 5 to 20 mg/g (Littke et al., 1995; Jurisch et al., 2012), and the N/TOC ratios range mainly between 0.01 and 0.02 (Fig. 3). Thus, the greater N_{tot}/TOC values (0.0463–0.0787, Fig. 3) for the three shale samples indicate significant contribution of inorganic nitrogen (Jurisch et al., 2012). According to the difference between the N_{tot}/TOC ratios of shale samples and their kerogen N_{org}/TOC_k ratios, the Lower Cambrian shale sample YC2R contains more inorganic nitrogen than the Lower Silurian shale sample YC4R and the Mesoproterozoic Xiamaling shale sample J7R (Table 2).

4.2. Pyrolysis temperature and vitrinite reflectance

Due to the limited amount of solid residues after pyrolysis experiments of shale or kerogen samples, it is difficult to prepare polished blocks to measure the pyrobitumen reflectance. Moreover, the conversion of pyrobitumen reflectance to equivalent vitrinite reflectance (EqVRo) is also a complex task due to the various conversion equations proposed by different authors (Mastalerz et al., 2018). It is generally accepted that the thermal maturity of sedimentary organic matter or the rank of coal depends mainly on their thermal history (Waples, 1980; Sweeney and Burnham, 1990), and therefore, the EqVRo values of the shale or kerogen samples are represented by the vitrinite reflectance (VRo) values of the coal samples that have experienced the same pyrolysis procedure as shale or kerogen samples.

However, it is worthy to note that the measured VRo value of coal at 300 °C is 0.69%, smaller than the original EqVRo value of the Xiamaling shale sample J7R (0.71%). This is caused by the smaller original Ro value of coal sample (0.56%), and therefore the real EqVRo value for the Xiamaling shale J7R at 300 °C is 0.71% rather than 0.69%. Thus, within the pyrolysis temperature range used in this study (Fig. 4), the EqVRo values of overmature shale samples YC2R and YC4R and their corresponding kerogen samples are in the range of 3.0–4.9%, whereas they vary between 0.71 and 4.9% for the Xiamaling shale sample J7R and its kerogen sample.

Table 2
Geochemical data of the three shales and their kerogens used for pyrolysis experiments.

Shale								Kerogen			
	Formation	Lithology	Mean bitumen reflectance (%)	TOC (wt. %)	N_{tot} (mg/g)	N_{inorg} [a] (mg/g)	N_{tot}/TOC		TOC_k [b] (wt. %)	N_{org} [c] (mg/g)	N_{org}/TOC_k
YC2R	Lower Cambrian Shuijingtuo Formation	Black shale	2.85	3.19	2.51	1.91	0.0787	YC2K	49.08	9.25	0.0188
YC4R	Lower Silurian Longmaxi Formation	Black shale	3.04	3.35	1.55	1.01	0.0463	YC4K	47.82	7.76	0.0162
J7R	Mesoproterozoic Xiamaling Formation	Black shale	0.74	3.26	1.52	0.88	0.0466	J7K	60.41	11.84	0.0196

[a] N_{inorg}: inorganic nitrogen content of shale sample; The N_{inorg} values were calculated by the following formula: $N_{inorg} = N_{tot} - N_{org}/TOC_k \times TOC_{shale}$.
[b] TOC_k: total organic carbon content of kerogen sample.
[c] N_{org}: organic nitrogen content of kerogen sample.

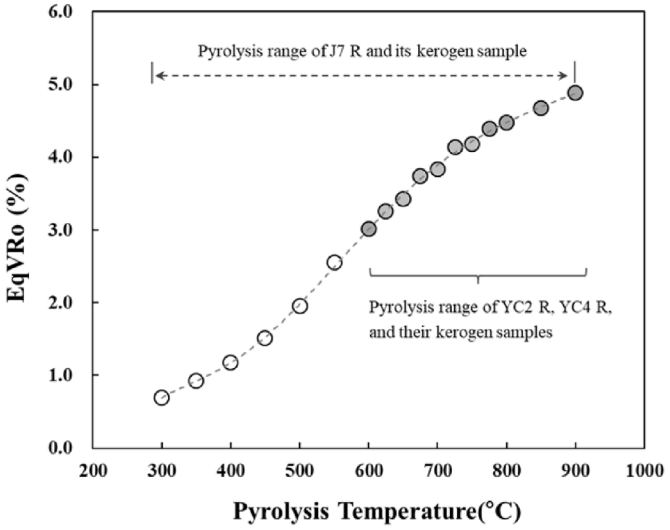

Fig. 4. Changes of equivalent vitrinite reflectance (EqVRo) values of shale samples with pyrolysis temperatures. The EqVRo values are equivalent to the measured vitrinite reflectance (VRo) values of vitrinite-rich coal samples at different pyrolysis temperatures except for the temperature of 300 °C at which the measured VRo value is 0.69%, smaller than the real EqVRo value of 0.71% for the Xiamaling shale sample (J7R) (see details in text).

4.3. Gas yields in pyrolysis experiments

4.3.1. Pyrolytic liberation of methane

Fig. 5 shows the yields of methane generated from the three shales and their kerogen samples. The highest yield of methane is observed for the low-maturity Xiamaling shale (J7R), while the amount of methane generated from the two overmature shale samples YC2R and YC4R is quite limited (Table 3). In addition, the methane yield of all shale samples shows a decreasing trend (gray shadows in Fig. 5) after 650 °C (EqVRo = 3.4%). Previous studies also observed such a decreasing trend of methane yield at very high pyrolysis temperatures (Krooss et al., 1995; Littke et al., 1995; Heim et al., 2012; Jurisch et al., 2012). The decrease in the cumulative yield of methane during pyrolysis indicates that methane is cracked in the experimental system, i.e., methane decomposition into carbon and hydrogen (Reinoso, 1998; Muradov and Veziroglu, 2005; Lee et al., 2008). Due to the strong C–H bonds, noncatalytic thermal cracking of methane usually requires temperatures higher than 1100 °C, but the required temperature can be significantly reduced when catalyst is present (Muradov and Veziroglu, 2005; Lee et al., 2008), and carbonaceous materials usually play a catalytic role in methane decomposition (Reinoso, 1998; Lee et al., 2008). Given that kerogen contains a variety of complex carbonaceous structures, they may have played a catalytic role in rupturing the C–H bond of methane at very high pyrolysis temperatures, which is likely one of the reasons why methane starts to decompose at 650 °C in the present isothermal pyrolysis experiment.

4.3.2. Pyrolytic liberation of molecular nitrogen

In the present study, the measurable N_2 generation starts at 300 °C for the low-maturity shale J7R and at 600 °C for the overmature Lower Paleozoic shale samples; the N_2 yield of the three shale samples all increased rapidly after 650 °C and continued to 900 °C (Fig. 5). This is consistent with previous studies that the N_2 generation from shales or coals may continue to pyrolysis temperatures as high as 1100–1200 °C (Krooss et al., 1995; Littke et al., 1995; Heim et al., 2012; Jurisch et al., 2012). Because the molecular nitrogen yield increases continuously during pyrolysis and the methane yield decreases after 650 °C, the difference between the molecular nitrogen and methane yields gradually narrow. At temperatures greater than 800 °C, the molecular

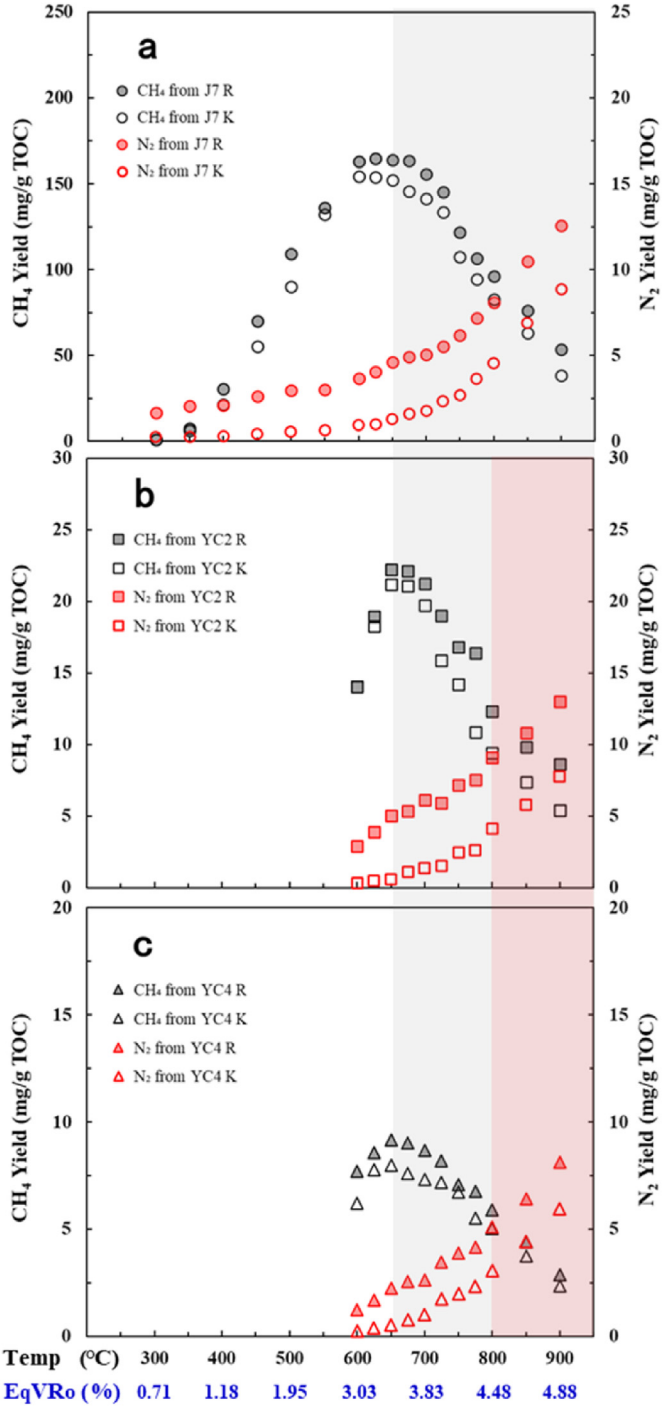

Fig. 5. Comparison of methane and molecular nitrogen yields of low-maturity shale J7R (a), overmature Lower Cambrian YC2R (b) and overmature Lower Silurian YC4R (c) as well as their kerogen samples. The gray-shaded zone indicates that the methane yield begins to decrease at temperatures above 650 °C, and the red-shaded part indicates that the nitrogen yield is higher than the methane yield above 800 °C. (For interpretation of the references to colour in this figure legend, the reader is referred to the Web version of this article.)

nitrogen yields of the overmature shale samples YC2R and YC4R exceed the methane yields (Fig. 5b and c). However, the methane yield of the low-maturity Xiamaling shale J7R is always higher than the molecular nitrogen yield, even above 800 °C (Fig. 5a).

Fig. 5 also reveals that the shale samples have much higher N_2 yields than their kerogen samples when the N_2 yields are normalized to TOC. Molecular nitrogen generated from shale samples during pyrolysis

Table 3
Yields of methane and molecular nitrogen generated from the shales and corresponding kerogen samples and the nitrogen and TOC contents in the solid residues after pyrolysis experiments.

Temperature	EqVRo	CH_4	N_2	N_2	N_{tot}	TOC	N_{tot}/TOC	CH_4	N_2	N_2	N_{org}	TOC_k	N_{org}/TOC_k
(°C)	(%)	mg/g TOC	mg/g TOC	mg/g N_{tot}	mg/g shale	wt.%		mg/g TOC_k	mg/g TOC_k	mg/g N_{org}	mg/g kerogen	wt.%	
		Sample J7R						Sample J7K					
300	0.71	0.91	1.68	36.06	1.52	3.26	0.047	1.25	0.27	13.80	11.84	60.24	0.020
350	0.93	7.56	2.06	44.11	1.52	2.98	0.051	6.44	0.26	13.29	12.06	60.83	0.020
400	1.18	30.61	2.10	45.10	1.49	2.81	0.053	21.40	0.32	16.28	12.61	61.04	0.021
450	1.51	70.25	2.61	56.08	1.52	2.78	0.055	55.50	0.42	21.18	11.88	62.22	0.019
500	1.95	109.40	2.96	63.59	1.31	2.83	0.046	90.25	0.57	29.25	11.66	62.88	0.019
550	2.55	136.23	3.02	64.86	1.07	2.83	0.038	132.24	0.65	33.25	11.34	62.03	0.018
600	3.03	162.84	3.68	78.95	0.85	2.88	0.030	154.23	0.98	49.79	11.09	61.50	0.018
625	3.26	164.72	4.08	87.50	0.80	2.83	0.028	154.08	1.01	51.50	10.58	59.84	0.018
650	3.42	163.75	4.63	99.34	0.68	2.83	0.024	152.10	1.30	66.32	9.81	59.32	0.017
675	3.74	163.49	4.91	105.26	0.70	2.81	0.025	145.47	1.60	81.38	9.28	58.81	0.016
700	3.83	155.58	5.06	108.55	0.64	2.65	0.024	141.12	1.77	90.32	8.98	58.08	0.015
725	4.14	145.44	5.52	118.42	0.61	2.76	0.022	133.51	2.10	107.27	8.24	57.61	0.014
750	4.18	121.77	6.20	132.89	0.56	2.52	0.022	107.41	2.70	137.72	8.02	55.17	0.015
775	4.39	106.65	7.18	153.95	0.61	2.44	0.025	94.55	3.64	185.69	7.64	55.39	0.014
800	4.48	96.03	8.10	173.68	0.49	2.27	0.022	82.59	4.57	233.27	6.94	54.62	0.013
850	4.67	76.23	10.49	225.00	0.45	1.90	0.024	63.39	6.88	351.16	6.35	53.74	0.012
900	4.88	53.50	12.58	269.74	0.41	1.74	0.024	38.40	8.87	452.31	5.95	53.91	0.011
		Sample YC2R						Sample YC2K					
600	3.03	14.04	2.88	36.63	2.51	3.19	0.079	14.03	0.31	16.67	9.10	49.03	0.019
625	3.26	18.93	3.90	49.61	2.23	3.25	0.069	18.25	0.46	24.36	8.91	48.64	0.018
650	3.42	22.21	5.05	64.20	1.80	3.11	0.058	21.20	0.55	29.37	8.14	48.35	0.017
675	3.74	22.14	5.35	67.96	1.62	2.96	0.055	21.10	1.08	57.30	8.12	47.94	0.017
700	3.83	21.24	6.11	77.69	1.58	2.86	0.055	19.71	1.36	72.39	7.26	47.74	0.015
725	4.14	19.00	5.92	75.26	1.41	2.68	0.053	15.88	1.53	81.43	7.20	47.96	0.015
750	4.18	16.79	7.17	91.18	1.33	2.55	0.052	14.19	2.47	131.31	7.10	47.50	0.015
775	4.39	16.39	7.52	95.62	1.25	2.18	0.057	10.85	2.62	139.26	6.24	47.19	0.013
800	4.48	12.33	9.09	115.54	1.18	2.26	0.052	9.41	4.12	218.47	5.98	45.93	0.013
850	4.67	9.81	10.82	137.45	1.05	1.94	0.054	7.40	5.77	306.12	5.51	45.31	0.012
900	4.88	8.64	13.01	165.34	0.94	1.66	0.057	5.39	7.74	410.83	5.22	45.27	0.012
		Sample YC4R						Sample YC4K					
600	3.03	8.57	1.24	26.79	1.54	3.20	0.048	6.94	0.25	15.47	7.40	48.46	0.015
625	3.26	9.55	1.70	36.77	1.51	3.15	0.048	8.68	0.38	23.43	7.48	47.12	0.016
650	3.42	10.20	2.26	48.90	1.21	3.07	0.039	8.89	0.54	33.16	6.76	47.31	0.014
675	3.74	10.07	2.57	55.46	1.15	2.84	0.040	8.49	0.78	48.18	6.64	45.76	0.015
700	3.83	9.66	2.65	57.18	1.03	2.78	0.037	8.15	1.02	62.67	6.61	46.98	0.014
725	4.14	9.12	3.49	75.35	1.00	2.75	0.036	8.00	1.76	108.33	6.30	45.38	0.014
750	4.18	7.88	3.90	84.37	0.95	2.52	0.038	7.52	1.98	122.32	5.98	45.04	0.013
775	4.39	7.53	4.18	90.32	0.93	2.46	0.038	6.14	2.35	145.08	5.58	45.29	0.012
800	4.48	6.60	5.10	110.14	0.90	2.30	0.039	5.62	3.07	189.14	5.31	44.43	0.012
850	4.67	4.92	6.43	138.92	0.82	2.13	0.038	4.19	4.43	273.20	4.89	45.04	0.011
900	4.88	3.23	8.14	175.83	0.74	1.96	0.038	2.64	5.96	367.27	4.19	44.02	0.010

comes from both organic nitrogen in kerogen and inorganic nitrogen in minerals, whereas it is only generated from organic nitrogen in the case of kerogen (Jurisch et al., 2012). Therefore, the difference in molecular nitrogen yield (mg/g TOC) between shales and their corresponding kerogen samples can reflect the contribution of inorganic nitrogen. In the present study, the difference in N_2 yield between the Lower Cambrian shale sample (YC2R) and its kerogen (YC2K) is from 2.6 to 5.3 mg/g TOC, whereas the difference for the Lower Silurian shale sample (YC4R) and its kerogen (YC4K) is only 0.8–2.2 mg/g TOC during pyrolysis (Table 3). Therefore, the contribution of inorganic nitrogen to the molecular nitrogen generation of Lower Cambrian shale is greater than that of the Lower Silurian shale. This is consistent with the fact that the inorganic nitrogen content of YC2R is significantly higher than that of YC4R (Table 2).

Fig. 6 further compares the molecular nitrogen yields normalized to specific nitrogen species among different samples. The total N_2 yields of the low-maturity shale sample J7R increase slowly from 36.1 to 99.3 mg/g N_{tot} at 300–650 °C (Fig. 6a). A rapid growth of N_2 generation for shale J7R is observed in the temperature range of 650–900 °C, and the maximum N_2 yield is 269.7 mg/g N_{tot} at the highest pyrolysis temperature. The N_2 yields of the two overmature shale samples YC2R and YC4R also increase with increasing pyrolysis temperature. At 900 °C, the total N_2 yields of shale samples YC2R and YC4R are 165.3 and 175.8 mg/g N_{tot} (Table 3), respectively. Therefore, the N_2 generation potential of overmature shale samples is significantly lower than that of the low-maturity shale sample, which indicates that a certain fraction of molecular nitrogen has been generated and released from the present overmature shales during their early maturation stage (Littke et al., 1995).

The molecular nitrogen generation curves of the three kerogen samples are quite similar at 650–900 °C, below which the cumulative yield of molecular nitrogen for the low-maturity kerogen J7K increases slowly with increasing temperature and is only 66.3 mg/g N_{org} at 650 °C (Fig. 6b). This indicates that the contribution of organic nitrogen to N_2 generation is limited before EqVRo evolves to 3.4%. At 900 °C, the maximum N_2 yields of the kerogen samples J7K, YC2K, and YC4K are 452.3, 410.8, and 367.3 mg/g N_{org} (Table 3), respectively. Based on the experimental results, the amount of N_2 generated from inorganic nitrogen in shale samples was calculated by deducting the amount of N_2 generated by kerogen (Fig. 6b) from the amount of N_2 generated by shale (Fig. 6a) according to nitrogen mass balance of the shale samples (Table 2). The results show that the N_2 generation from the inorganic nitrogen fraction in all the three shales is relatively rapid before 650 °C compared to the sluggish increase at further elevated temperatures (Fig. 6c); in addition, at temperatures greater than 700–725 °C, the inorganic N_2 yields (mg/g N_{inorg}) become much lower than the organic

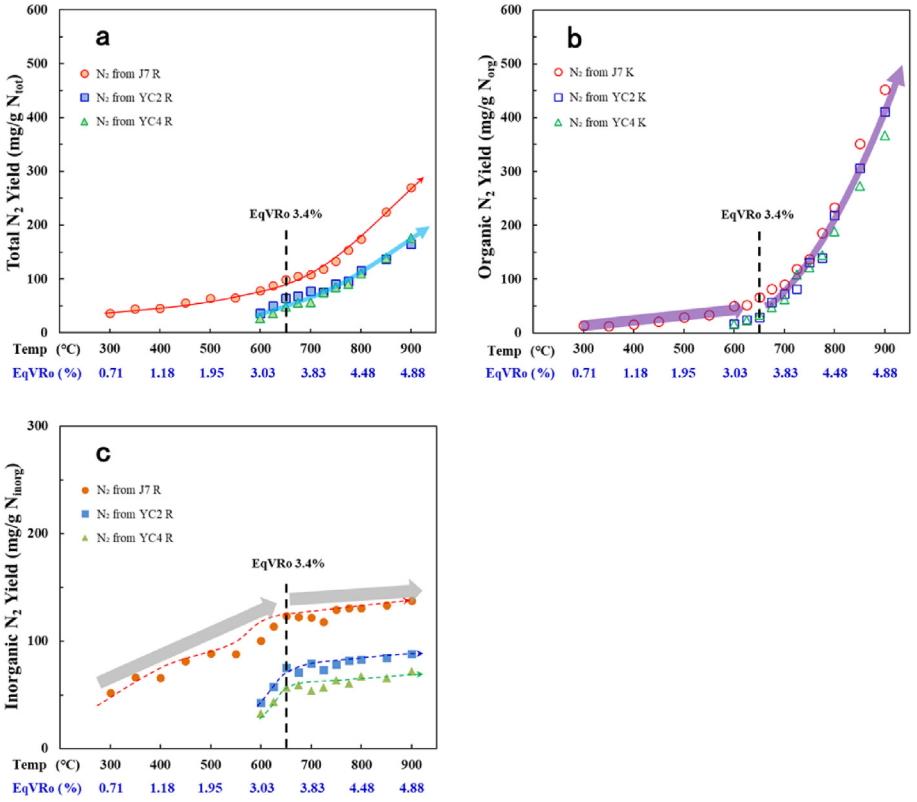

Fig. 6. Comparison of total (a), organic (b) and inorganic (c) molecular nitrogen (N_2) yields during pyrolysis. The yields of inorganic N_2 were calculated by mass balance with the following formula: $N_{2(inorg)} = (N_{2(tot)} \times N_{tot}\text{-}N_{2(org)} \times N_{org}/TOC_k \times TOC_{shale})/N_{inorg}$. The organic N_2 yields of kerogen samples increase rapidly only above 650 °C and then exceed the inorganic N_2 yields of shales at temperatures greater than 700–725 °C, indicating a higher conversion of elemental nitrogen to molecular nitrogen in the case of kerogen.

N_2 yields (mg/g N_{org}), indicating the N_2 generated from shales at very high maturity would be dominated by organic N_2 if the inorganic and organic nitrogen contents are similar in shales.

4.4. Evolution of TOC and nitrogen contents during pyrolysis

4.4.1. Changes of nitrogen and TOC contents

Progressive maturation of organic matter up to metamorphism affects the concentration of organic and inorganic nitrogen species in different ways (Boudou et al., 2008; Jurisch et al., 2012). The changes of nitrogen contents with pyrolysis temperatures in shale and kerogen samples are plotted in Fig. 7. It is evident that the evolutional trends of nitrogen content are distinct at different pyrolysis stages, which is true of both the N_{tot} in shales and organic nitrogen in kerogens. The N_{tot} abundance of the low-maturity Xiamaling shale J7R shows no obvious change at the early stage of pyrolysis (300–450 °C) and then decreases rapidly from 1.52 to 0.68 mg/g shale at 450–650 °C. With increasing pyrolysis temperature, the N_{tot} decreases continuously and becomes as low as 0.41 mg/g shale at 900 °C (Fig. 7a). The N_{tot} values of the two overmature shale samples YC2R and YC4R also decrease continuously during pyrolysis. From 600 to 900 °C, the N_{tot} values of the Lower Cambrian shale YC2R drop from 2.51 to 0.94 mg/g shale, while they decrease from 1.54 to 0.74 mg/g shale for the Lower Silurian shale YC4R (Fig. 7a).

In general, the changes of nitrogen content of kerogen samples are similar to those of their shale samples. The nitrogen content of the kerogen sample J7K does not change much before 600 °C, after which it begins to decrease with increasing pyrolysis temperatures. The changes of nitrogen contents with pyrolysis temperature for kerogens YC2K and YC4K are similar to those of kerogen J7 K at the 600–900 °C (Fig. 7b). For example, at the temperature range of 600–900 °C, the kerogen nitrogen content decreases from 11.09 to 5.95 mg/g kerogen for sample J7K, from 9.10 to 5.22 mg/g kerogen for sample YC2K, and from 7.40 to 4.19 mg/g kerogen for sample YC4K (Fig. 7b; Table 3). One reason for this similarity in the changes of nitrogen contents during pyrolysis for the three kerogen samples is likely that they contain species of organic nitrogen that have similar thermal stability. Based on mass balance, the inorganic nitrogen contents (N_{inorg}) in residual shale samples after pyrolysis were also calculated, and their evolutional trends with pyrolysis temperature are presented in Fig. 7c, illustrating that they are similar to those of total nitrogen contents and display a rapid decrease in 450–650 °C followed by a sluggish reduction in 650–900 °C.

The TOC contents of the low-maturity Xiamaling shale J7R decrease quickly from 3.26 to 2.81% at the initial stage of pyrolysis (300–400 °C) and then keep largely constant at the 450–650 °C, after which they decrease again and finally lower to 1.74% at 900 °C (Table 3). The TOC contents of the two overmature shale samples YC2R and YC4R decrease continuously during pyrolysis. From 600 to 900 °C, the TOC contents of Lower Cambrian shale YC2R drops from 3.19 to 1.66%, while they decrease from 3.20 to 1.96% for the Lower Silurian shale YC4R (Table 3).

The TOC content of kerogen sample J7K changes little at 300–600 °C and then decreases continuously with increasing pyrolysis temperature. Similarly, the TOC contents of the kerogens YC2K and YC4K also decrease continuously at 600–900 °C. For example, from 600 to 900 °C, the TOC values of kerogen J7K decrease from 61.50 to 53.91%, from 49.03 to 45.27% for the kerogen YC2K and from 48.46 to 44.02% for the kerogen YC4K (Table 3).

4.4.2. N/TOC ratios for different samples

Based on the analytical dataset, we also attempted to identify the systematic variations in N/TOC ratios with pyrolysis temperature. Early studies reveal that N/TOC ratios of coals and carbonaceous rocks range between 0.01 and 0.02 (Littke et al., 1995; Boudou et al., 2008; Mavridou et al., 2008; Heim et al., 2012), while those of shales range from 0.01 to 0.39 and show only a slight dependence on depositional environments (Jurisch et al., 2012). The relationships between N_{tot} and TOC contents for our three shales at different pyrolysis temperatures are shown in Fig. 8a. It is evident that the relationships between N_{tot} and TOC values for the low-maturity shale J7R are obviously distinct

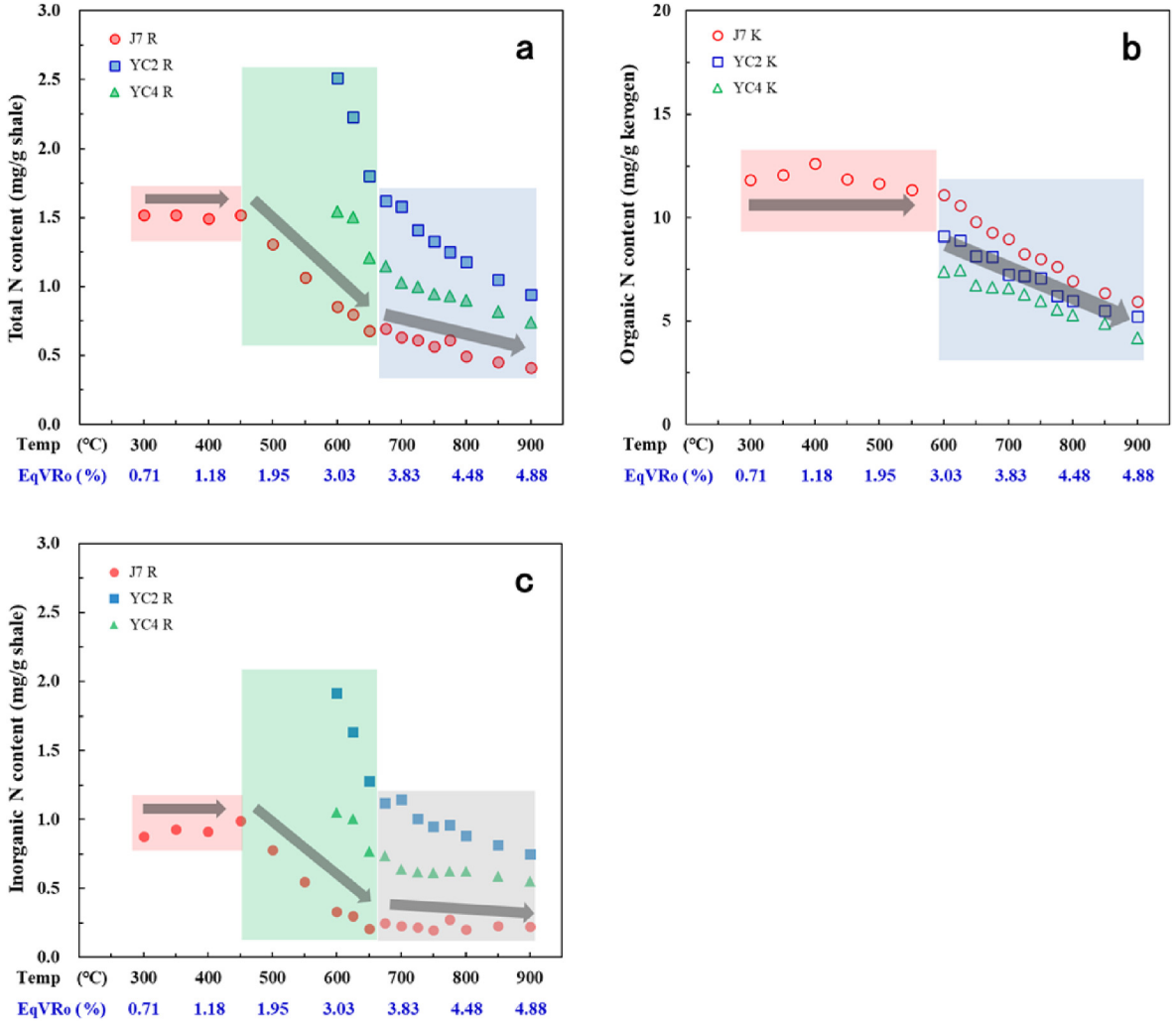

Fig. 7. Change in nitrogen contents for the three black shales and their kerogen samples during pyrolysis. (a) The changes of total nitrogen content in shales (N_{tot}) can be divided into three stages: almost no change below 450 ˚C, a rapid decline from 450 to 650 ˚C and a slower decrease above 650 ˚C. The organic nitrogen content in kerogen (N_{org}) fluctuates before 600 ˚C and then gradually decreases above 600 ˚C (b). The evolutional trends of inorganic nitrogen contents (N_{inorg}) are similar to those of total nitrogen contents, showing a rapid decrease in 450–650 ˚C followed by a sluggish reduction in 650–900 ˚C (c).

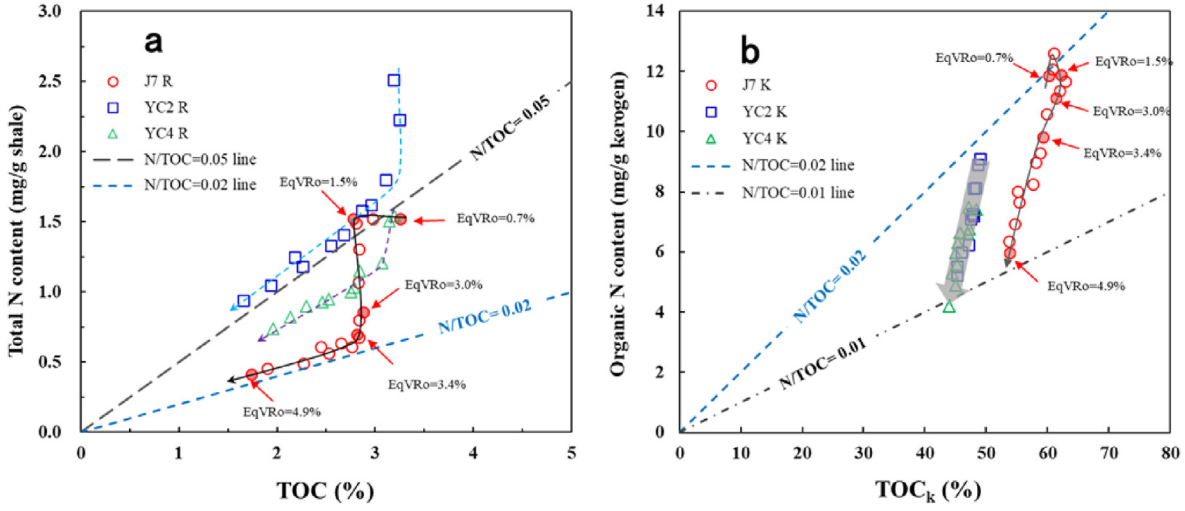

Fig. 8. Relationship between nitrogen and TOC contents in shales and kerogens during pyrolysis. The different trends of N-TOC relationships between shale and kerogen samples reflect their different releasing processes due to the presence or absence of inorganic nitrogen.

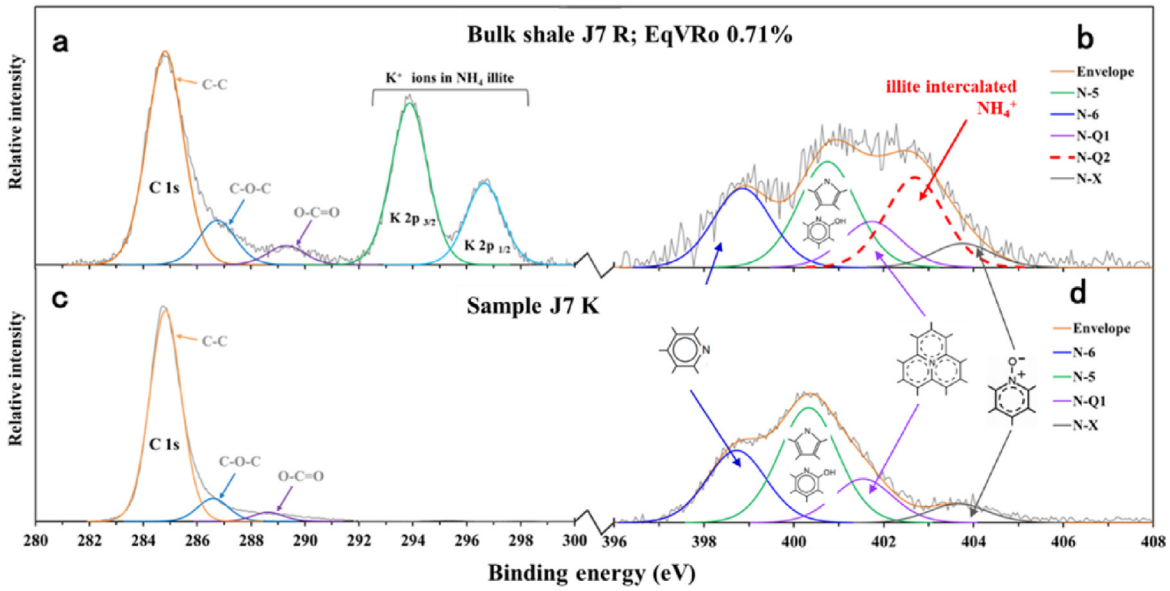

Fig. 9. N 1s XPS and C 1s XPS spectra with curve-fitted subpeaks for the Xiamaling shale sample J7R that contains ammonium illite (a and b) and its corresponding kerogen sample J7K (c and d). The N 1s XPS spectra shale sample J7 R (b) features an N-Q2 subpeak at approximately 402.7 eV, unlike the kerogen J7 K spectra (d); thus, the N-Q2 subpeak can reflect the characteristics of inorganic nitrogen in shales, which has been confirmed in previous studies (Daniels and Altaner, 1993; Boudou et al., 2008). Organic nitrogen is usually reflected by subpeaks of N-6, N-5, N-Q1, and N-X XPS (b and d), which are pyridinic nitrogen, pyrrolic or pyridinic nitrogen, quaternary nitrogen, and nitrogen oxide, respectively (see details in Boudou et al., 2008).

during different pyrolysis stages. At the initial pyrolysis stage (EqVRo = 0.7–1.5%), the TOC content of shale J7R decreases with maturation but only minor changes are observed for N_{tot} content, leading to an increased N_{tot}/TOC ratios at this stage (Table 3); however, at the thermal evolution stage of EqVRo = 1.5–3.4%, the TOC values change little but the N_{tot} values are reduced significantly, resulting in a sharp increase in the N_{tot}/TOC ratios of shale J7R from 0.055 to 0.026 (Table 3); at late pyrolysis (EqVRo > 3.4%), both the TOC and N_{tot} contents of shale J7R both decrease, and therefore the N_{tot}/TOC ratios are largely unchanged. In summary, the relations between N_{tot} and TOC contents of the low-maturity shale J7R are divided into three stages over the whole thermal evolution process (Fig. 8a). Because the maturity of the other two shale samples YC2R and YC4R matched the late stage of dry gas generation (EqVRo ≈ 3.0%), the relations between N_{tot} and TOC contents of the two samples are similar to the relations in the second and third stages of low-maturity sample J7R in the N-TOC diagram, i.e., the N_{tot}/TOC ratios of YC2R and YC4R first decline rapidly at the of pyrolysis temperatures of 600–650 °C and then keep largely constant with minor changes (Table 3; Fig. 8a).

The N_{org}/TOC_k ratios for the three kerogen samples during pyrolysis are quite different from those of their corresponding shale samples (Fig. 8b). One of the distinct characteristics is that both the low-maturity kerogen J7K and the overmature kerogens YC2K and YC4K have N_{org}/TOC_k ratios in the range of 0.01–0.02 during the whole pyrolysis experiments. For kerogen sample J7K, both the TOC and organic nitrogen contents slightly first increase and then decrease during pyrolysis (Fig. 8b). The N_{org}/TOC_k ratios of the kerogen sample J7K vary around 0.02 at EqVRo = 0.7–1.5% and then decreases gradually with increasing thermal maturity, approximately approaching to 0.01 at the end of pyrolysis. Similarly, the N_{org}/TOC_k ratios of kerogen samples YC2K and YC4K also decrease gradually and approach to the value of 0.01 with increasing thermal maturity (Fig. 8b).

4.5. Evolution of nitrogen species during pyrolysis

4.5.1. Deconvolution of N 1s XPS spectra: subpeaks of inorganic and organic N

Chemical–structural assignments of N 1s XPS spectra were guided by known binding energies of nitrogen in model compounds and purified substrates (Pels et al., 1995; Casanovas et al., 1996; Gammon et al., 2003; Boudou et al., 2008). The chemical speciation of organic nitrogen (N_{org}) within organic matter changes with time and maturation during burial. Progressive thermal evolution of organic matter involves phases of enhanced elimination of N_{org} and ultimately produces graphite containing only traces of nitrogen (Boudou et al., 2008). Organic nitrogen species are usually identified by subpeaks of N-6, N-5, N-Q1, and N-X XPS (Fig. 9), corresponding to pyridinic nitrogen, pyrrolic or pyridinic nitrogen, quaternary nitrogen, and nitrogen oxide, respectively (Pels et al., 1995; Casanovas et al., 1996; Gammon et al., 2003; Boudou et al., 2008). Ammonium salts, such as ammonium illite and ammonium feldspar, are typical forms of inorganic nitrogen (Boudou et al., 2008; Dai et al., 2018). The N 1s XPS evidence for an ammonium is the subpeak N-Q2, which occurs at a relatively high binding energy and has been corroborated by previous studies (Buckley et al., 1995; Gong et al., 1999; Boudou et al., 2008).

No K 2p XPS peaks in the binding energy range of 293.7–296.7 eV are identified in our kerogen samples (Fig. 9c), indicating that there are no mineral-hosted ammonium. The N 1s XPS spectra of the shale sample J7R feature a N-Q2 Lorentzian–Gaussian subpeak at approximately 402.7 eV, which, however, is not identified in the spectra of kerogen J7K (Fig. 9 b, d). Previous studies have suggested that the N-Q2 subpeak reflects the ammonium in illite, which has been confirmed by XRD (Daniels and Altaner, 1993; Boudou et al., 2008). Therefore, subpeak N-Q2 can be used to investigate the changes in inorganic nitrogen content in shales during pyrolysis, whereas subpeaks N-6, N-5, N-Q1, and N-X indicate the structural characteristics of organic nitrogen (Boudou et al., 2008).

4.5.2. Inorganic nitrogen: changes in subpeak N-Q2

N 1s XPS spectra with curve-fitted subpeaks for the low-maturity shale J7R during pyrolysis process are shown in Fig. 10. One obvious feature is that the subpeak N-Q2 does not change significantly before 450 °C (Fig. 10b); however, its relative intensity declines rapidly from 450 to 650 °C (Fig. 10c) and then remains largely constant at further elevated temperatures (Fig. 10d).

Semi-quantitative XPS analysis shows that the relative intensity of

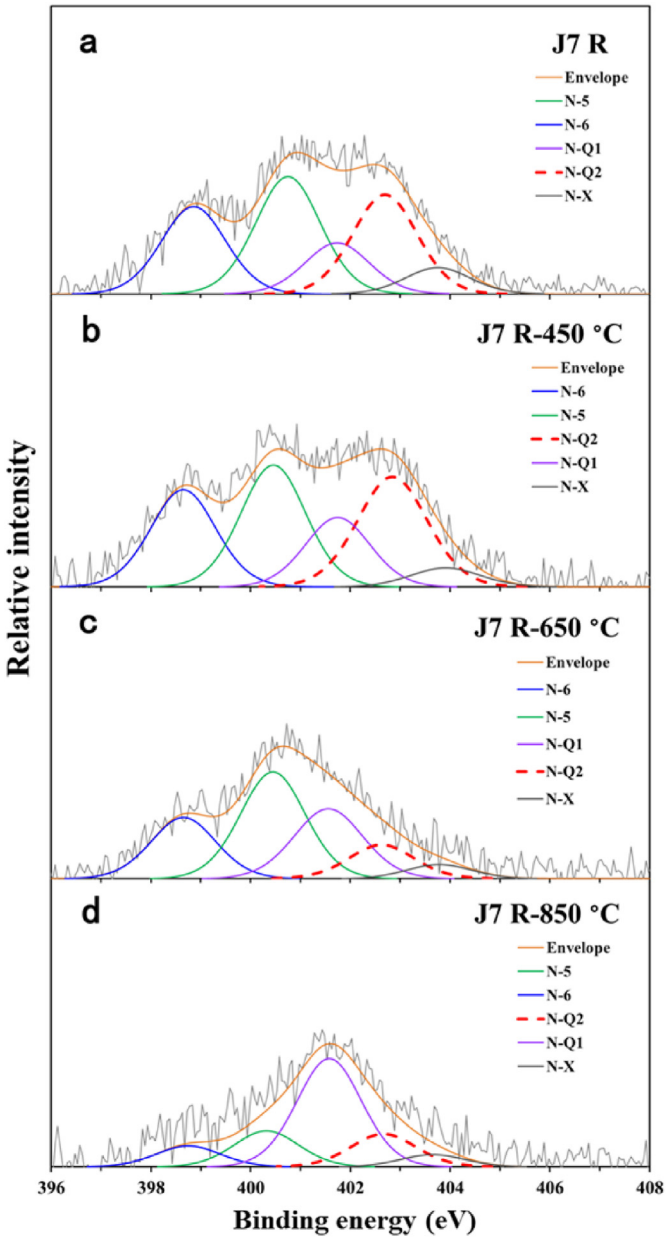

Fig. 10. N 1s XPS spectra with curve-fitted subpeaks for the low-maturity shale J7R in pyrolysis experiments. The relative intensity of the N-Q2 subpeak declines rapidly from 450 to 650 °C, indicating that inorganic nitrogen in shale is released in large quantities at this stage. An evident decrease in the relative intensity for subpeaks N-6 and N-5 and a significant increase in the N-Q1 subpeak at temperatures above 650 °C indicate that organic nitrogen has been released in large amounts.

the N-Q2 subpeak of the Lower Cambrian shale YC2R is obviously higher than the intensities of other subpeaks (Fig. 11a), but the N-Q2 subpeak of the Lower Silurian shale YC4R is not the highest peak of among the XPS subpeaks (Fig. 11d), which is consistent with the fact that the inorganic nitrogen content of shale YC2R is greater than that of shale YC4R (Table 2). Like the Xiamaling shale J7R, the relative intensities of the N-Q2 subpeak of the Lower Cambrian shale YC2R and the Lower Silurian shale YC4R were significantly reduced at 650 °C, after which they are only lowered in a minor extent (Fig. 11). In summary, the inorganic nitrogen in our shale samples is mainly released at temperatures before 650 °C, no matter the original content of inorganic nitrogen is high or low (Figs. 10 and 11).

4.5.3. Organic nitrogen: subpeaks N-6, N-5, N-Q1, and N-X

Subpeaks N-6, N-5, N-Q1, and N-X of the organic nitrogen correspond to nitrogen with mean binding energies of 398.8 eV, 400.3 eV, 401.6 eV, and 403.7 eV, respectively, when the maximum of the C 1s envelope is calibrated to 284.8 eV in this study. In the process of pyrolysis, the relative intensities of various subpeaks of organic nitrogen in Xiamaling shale keep largely constant below 450 °C (Fig. 10b), then followed by a reduction at higher temperatures (Fig. 10c); an evident decrease in subpeaks N-6 and N-5 is especially noticed, while the N-Q1 subpeak significantly increases in intensity after 650 °C (Fig. 10d). These observations indicate that the significant release of organic nitrogen begins at an EqVRo value of 3.4% and increases with increasing thermal maturity.

The chemical structures of organic nitrogen in overmature shale samples YC2R and YC4R vary quite similarly during pyrolysis. For example, except the relative intensity of the N-X subpeak decreases to a certain extent, the subpeaks N-6, N-5, and N-Q1 of shale YC4R and YC2R do not change much at 650 °C (Fig. 11 b, e). When the pyrolysis temperature reaches 850 °C, the subpeaks N-6, N-5, and N-X of shale YC4R and YC2R decrease strongly, whereas the subpeak N-Q1 increases significantly (Fig. 11 c, f), which is consistent with the results of Boudou et al. (2008) who attributed the increase of N-Q1 to either its selective preservation inside aromatic carbon lattices or neoformation in condensed ring systems.

4.5.4. Implications for release order of nitrogen of different species

The aforementioned results show that the timing of nitrogen release from different nitrogen structures is distinct during thermal evolution. According to the XPS characteristics of the three shale samples, the inorganic nitrogen, hosted mainly in ammonium minerals and represented by the N-Q2 subpeak, is released earlier than the organic nitrogen bound in kerogen (Figs. 10 and 11). In light of the results from the present pyrolysis results, the major reduction of N-Q2 subpeak occurs before 650 °C (Figs. 10 and 11), which is consistent with the generation profile of inorganic molecular nitrogen (Fig. 6c) and the rapid reduction of N/TOC ratios of bulk shale samples in the EqVRo range of 1.5–3.4% (Fig. 8a), and may indicate that the molecular nitrogen generated within the hydrocarbon gas window (EqVRo < 3.4%) is likely mainly derived from the release of inorganic nitrogen when the inorganic and organic nitrogen contents are comparable in shales.

After the major release of inorganic nitrogen (e.g., EqVRo > 3.4%), kerogen becomes increasingly aromatic, with smaller aromatic ring structures condensing to form larger polyaromatic clusters (Beyssac et al., 2002). At this time, the methane generation potential is exhausted and the kerogen samples continued to release the reactive nitrogen species which is primarily located along the edge of condensed and partially aromatic systems and characterized by the N-6 and N-5 subpeaks (Figs. 9–11). During this process, the yield of molecular nitrogen generated from kerogen samples (mg/g N_{org}) increases rapidly (Fig. 6b), indicating that the organic nitrogen in kerogen is mainly released as molecular nitrogen.

The above observations indicate that the molecular nitrogen associated with the process of methane formation (EqVRo < 3.4%) is preferentially derived from the inorganic nitrogen in ammonium-bearing minerals (Fig. 6 b, c), and therefore the potential of molecular nitrogen from a shale at this thermal maturity stage is mainly determined by the content of inorganic nitrogen. At EqVRo > 3.4%, the methane potential is exhausted and the organic nitrogen in kerogen begins to be released in large quantity, leading to the rapid generation of organic molecular nitrogen (Fig. 6b). Therefore, maturity level has a profound influence on the yield of molecular nitrogen derived from kerogen and exceptionally high maturity may increase the risk of molecular nitrogen. This is consistent with previous studies that natural gas with a high content of molecular nitrogen (> 50%) in the Northern German Basin is mainly derived from coal-bearing strata with Ro values

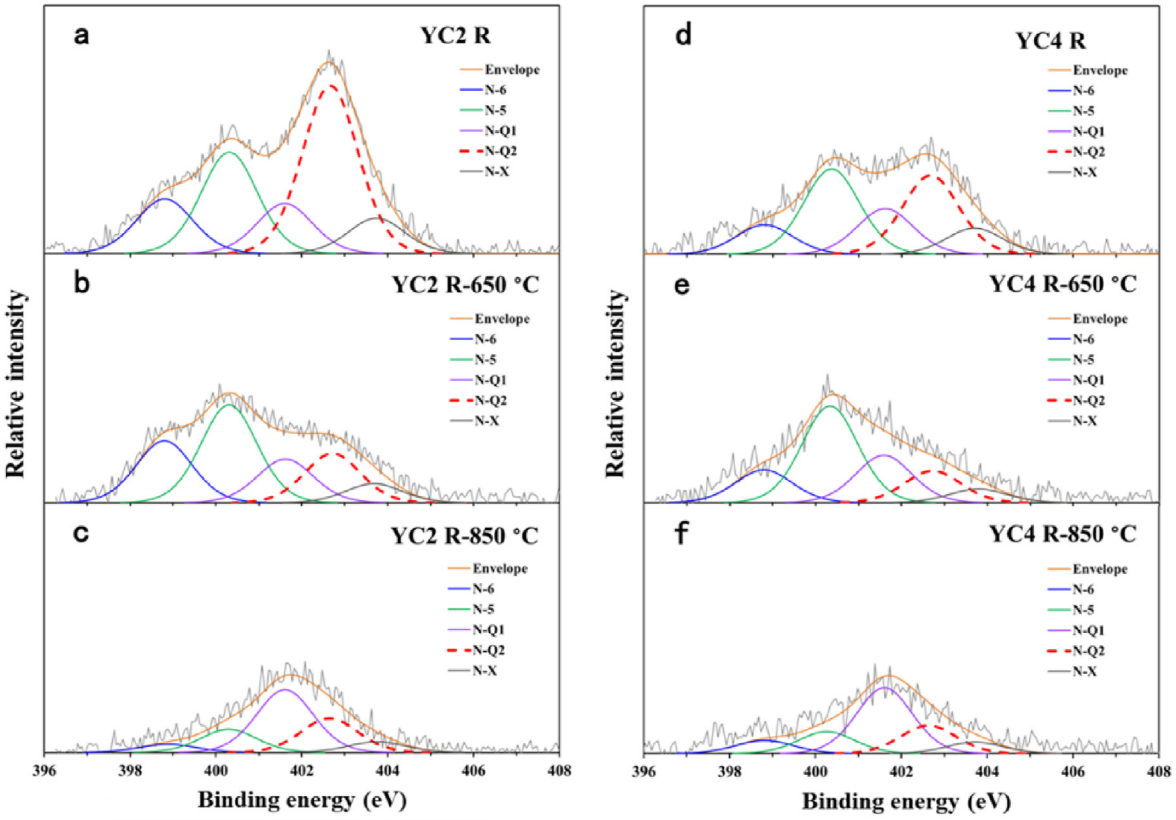

Fig. 11. N 1s XPS spectra with curve-fitted subpeaks for the two overmature shale samples YC2R and YC4R in pyrolysis experiments.

greater than 3.5% and very high organic matter content (Krooss et al., 1995). Similarly, the N_2-rich Lower Cambrian shale strata (greater than 90% on average, Jiao et al., 2017) in southern China are also organic-rich (average TOC > 7%) and have EqVRo values greater than 4.0% (Li et al., 2017). However, only a minor content of molecular nitrogen is present in the Lower Silurian shales (average content is less than 2.2%, see in Dai et al., 2014; Zhang et al., 2018), which have lower maturity and lower TOC content than the Lower Cambrian shales (Zou et al., 2010; Tian et al., 2013; Dai et al., 2014, 2016; Pan et al., 2016). Therefore, source rocks with exceptionally high maturity and a high abundance of organic nitrogen likely indicate high molecular nitrogen risk. In addition, the preservation conditions of shale gas also have an influence on its composition because high contents of molecular nitrogen in southern China were mostly encountered in regions where deep-seated faults are extended to surface (Su et al., 2019; Wu et al., 2019). In such cases, the early generated methane may be lost to various extents and the shale reservoirs would be recharged with the late-generated N_2-rich gas at EqVRo > 3.4% stage. Moreover, the addition of molecular nitrogen into the shale gas may accelerate methane desorption by reducing its partial pressure, especially when the shale reservoirs are characterized with fractures and have high permeability (Bustin et al., 2016; Li and Elsworth, 2019), further leading to the relative enrichment of molecular nitrogen. In summary, when the molecular nitrogen risk is taken into account during overmature shale gas exploration in regions of complex tectonic history, the upper limit of shale maturity for successful shale gas exploration may need to be specifically assessed in terms of the generation potential of molecular nitrogen from different nitrogen species in shales.

5. Conclusions

Two overmature Lower Paleozoic black shales and one low-maturity shale with similar kerogen type and TOC content but different nitrogen compositions were used to investigate the nitrogen release during pyrolysis experiments. Based on the experimental results, the characteristics of molecular nitrogen generation from different nitrogen species and the molecular nitrogen risk of overmature Lower Paleozoic black shales were tentatively discussed. The main conclusions are summarized below.

(1) The maximum molecular nitrogen yields at EqVRo = 4.9%, normalized to total nitrogen content (N_{tot}), of the two overmature shales (EqVRo = 2.85–3.04%) vary between 165 and 176 mg/g N_{tot}, approximately 61–65% of those for the low-maturity shale (EqVRo = 0.7%). This indicates that the overmature shales have released nitrogen in geological history but still have great potential of molecular nitrogen generation at higher thermal maturity levels.
(2) Thermal maturity is the main controlling factor for molecular nitrogen release from kerogen. The amount of molecular nitrogen from kerogen is limited within methane generation stage (EqVRo < 3.4%), but begins to increase rapidly at EqVRo values greater than 3.4%, illustrating that the main formation stage of molecular nitrogen from Type II marine kerogen is consistent with type III kerogen (Krooss et al., 1995).
(3) Different from the generation of molecular nitrogen from kerogen, the molecular nitrogen generation from ammonium-bearing minerals in the present experimental conditions mainly occurs at EqVRo values smaller than 3.4%, and it generation potential in the EqVRo range of 3.4–4.9% becomes quite limited. In addition, at the maximum experimental thermal maturity (EqVRo = 4.9%), the inorganic molecular nitrogen yield (mg/g N_{inorg}) is much lower than the organic molecular nitrogen yield (mg/g N_{org}), which further indicates that exceptionally high maturity and high abundance of organic nitrogen are likely the main controls on the high content of molecular nitrogen in Lower Cambrian shales in South China.

CRediT authorship contribution statement

Haifeng Gai: Conceptualization, Validation, Formal analysis, Writing - original draft. **Hui Tian:** Conceptualization, Writing - review & editing, Resources, Supervision. **Peng Cheng:** Validation, Visualization. **Chunmin He:** Investigation. **Zijin Wu:** Visualization. **Sui Ji:** Data curation. **Xianming Xiao:** Resources.

Declaration of competing interest

The authors declare that they have no known competing financial interests or personal relationships that could have appeared to influence the work reported in this paper.

Acknowledgments

This study was jointly supported by the Natural Science Foundation of China (Grant No. 41925014, 4160304, and 41522302), the National Science and Technology Major Project (2017zx05008-002-004) and GIG "135" project (135TP201602). This is contribution No.IS-2875 from GIGCAS.

Nomenclature

N_{tot}	total nitrogen content
N_{org}	organic nitrogen content
N_{inorg}	inorganic nitrogen content
TOC	total organic carbon content of shale
TOC_k	total organic carbon content of kerogen
VRo	vitrinite reflectance measured from the vitrinite-rich coal sample
EqVRo	equivalent vitrinite reflectance
N-6	pyridinic nitrogen atom in an aromatic ring
N-5	pyrrolic nitrogen atom in a non-aromatic ring, or pyridinic nitrogen atom in rings bearing oxygen-containing substituents
N-Q1	quaternary nitrogen, a nitrogen atom is bonded to three carbon atoms within a condensed, partially aromatic system
N-Q2	inorganic nitrogen fixed in ammonium-bearing minerals
N-X	nitrogen oxide

References

Algeo, T.J., Rowe, H., Hower, J.C., Schwark, L., Herrmann, A., Heckel, P., 2008. Changes in ocean denitrification during Late Carboniferous glacial-interglacial cycles. Nat. Geosci. 1, 709–714.
Allègre, C.J., Staudacher, T., Sarda, P., 1987. Rare gas systematics: formation of the atmosphere, evolution and structure of the Earth's mantle. Earth Planet Sci. Lett. 81, 127–150.
Andersen, T., Austrheim, H., Burke, E.A.J., Elvevold, S., 1993. N_2 and CO_2 in deep crustal fluids: evidence from the Caledonides of Norway. Chem. Geol. 108, 113–132.
Baxby, M., Patience, R.L., Battle, K.D., 1994. The origin and diagenesis of sedimentary organic nitrogen. J. Petrol. Geol. 17 (2), 211–230.
Behar, F., Gillaizeau, B., Derenne, S., Largeau, C., 2000. Nitrogen distribution in the pyrolysis products of a type II kerogen (Cenomanian, Italy): timing of molecular nitrogen production versus other gases. Energy Fuels 14 (2), 431–440.
Beyssac, O., Rouzaud, J.N., Goffé, B., Brunet, F., Chopin, C., 2002. Graphitization in a high pressure low-temperature metamorphic gradient: a Raman microspectroscopy and HRTEM study. Contrib. Mineral. Petrol. 143, 19–31.
Boudou, J.P., Espitalié, J., 1995. Molecular nitrogen from coal pyrolysis: kinetic modelling. Chem. Geol. 126, 319–333.
Boudou, J.P., Schimmelmann, A., Ader, M., Masterlerz, M., Sebilo, M., Gengembre, L., 2008. Organic nitrogen chemistry during low-grade metamorphism. Geochem. Cosmochim. Acta 72, 1199–1221.
Boyd, S.R., 2001. Nitrogen in future biosphere studies. Chem. Geol. 176, 1–30.
Brandes, J.A., Devol, A.H., Deutsch, C., 2007. New developments in the marine nitrogen cycle. Chem. Rev. 107 (2), 577–589.
Buckley, A.N., Kelly, M.D., Nelson, P.F., Riley, K.W., 1995. Inorganic nitrogen in Australian semi-anthracites; implications for determining organic nitrogen functionality in bituminous coals by X-ray photoelectron spectroscopy. Fuel Process. Technol. 43, 47–60.
Busigny, V., Lebeau, O., Ader, M., Krapez, B., Bekker, A., 2013. Nitrogen cycle in the Late Archean ferruginous ocean. Chem. Geol. 362, 115–130.
Bustin, A.M.M., Bustina, R.M., Chikatamarla, L., Downey, R., Mansoori, J., 2016. Learnings from a failed nitrogen enhanced coalbed methane pilot: piceance Basin, Colorado. Int. J. Coal Geol. 165, 64–75.
Canfield, D.E., Glazer, A.N., Falkowski, P.G., 2010. The evolution and future of Earth's nitrogen cycle. Science 330, 192–196.
Casanovas, J., Ricart, J.M., Rubio, J., Illas, F., Jimenez-Mateos, J.M., 1996. Origin of the large N 1s binding energy in X-ray photoelectron spectra of calcined carbonaceous materials. J. Am. Chem. Soc. 118, 8071–8076.
Chen, J., Xiao, X., 2014. Evolution of nanoporosity in organic-rich shales during thermal maturation. Fuel 129, 173–181.
Chen, J.F., Zhu, Y.N., 2003. The origin of molecular nitrogen in natural gas and geochemical characters of molecular nitrogen in natural gas from east part of Tarim Basin. Nat. Gas Geosci. 14, 172–176 (in Chinese with English abstract).
Dai, J., Chen, H., Shen, X., 2005. Geochemistry and occurrence of inorganic gas accumulations in Chinese sedimentary basins. Org. Geochem. 36, 1664–1688.
Dai, J.X., 1992. Identification and distinction of various alkane gases. Sci. China Ser. B Earth Sci. 35, 1246–1257.
Dai, J.X., Zou, C.N., Liao, S.M., Dong, D.Z., Ni, Y.Y., Huang, J.L., Wu, W., Gong, D.Y., Huang, S.P., Hu, G.Y., 2014. Geochemistry of the extremely high thermal maturity Longmaxi shale gas, southern Sichuan Basin. Org. Geochem. 74, 3–12.
Dai, J.X., Zou, C.N., Dong, D.Z., Ni, Y.Y., Wu, W., Gong, D.Y., Wang, Y.M., Huang, S.P., Huang, J.L., Fang, C.C., Liu, D., 2016. Geochemical characteristics of marine and terrestrial shale gas in China. Mar. Petrol. Geol. 76, 444–463.
Dai, S.F., Xie, P.P., David, F., Ward, C.R., Graham, I.T., Yan, X.Y., 2018. The occurrence of buddingtonite in super-high-organic-sulphur coals from the Yishan coalfield, Guangxi, southern China. Int. J. Coal Geol. 195, 347–361.
Daniels, E.J., Altaner, S.P., 1993. Inorganic nitrogen in anthracite from eastern Pennsylvania, USA. Int. J. Coal Geol. 22, 21–35.
Deutsch, C., Sarmiento, J.L., Sigman, D.M., Gruber, N., Dunne, J.P., 2007. Spatial coupling of nitrogen inputs and losses in the ocean. Nature 445, 163–167.
Falkowski, P.G., 1997. Evolution of the nitrogen cycle and its influence on the biological sequestration of CO_2 in the ocean. Nature 387, 272–275.
Gammon, W.J., Kraft, O., Reilly, A.C., Holloway, B.C., 2003. Experimental comparison of N(1s) X-ray photoelectron spectroscopy binding energies of hard and elastic amorphous carbon nitride films with reference organic compounds. Carbon 41, 1917–1923.
Ghalandari, V., Hashemipour, H., Bagheri, H., 2020. Experimental and modeling investigation of adsorption equilibrium of CH_4, CO_2, and N_2 on activated carbon and prediction of multicomponent adsorption equilibrium. Fluid Phase Equil. 208, 112433.
Gold, T., Held, M., 1987. Helium-nitrogen-methane systematics in natural gases of Texas and Kansas. J. Petrol. Geol. 10 (4), 415–424.
Gong, B., Buckley, A.N., Lamb, R.N., Nelson, P.F., 1999. XPS determination of the forms of nitrogen in coal pyrolysis chars. Surf. Interface Anal. 28, 126–130.
Hao, F., Zou, H., Lu, Y., 2013. Mechanisms of shale gas storage: implications for shale gas exploration in China. AAPG Bull. 97, 1325–1346.
Heim, S., Jurisch, S.A., Krooss, B.M., Weniger, P., Littke, R., 2012. Systematics of pyrolytic N_2 and CH4 release from peat and coals of different thermal maturity. Int. J. Coal Geol. 89, 84–94.
Jarvie, D.M., Claxton, B.L., Henk, F., Breyer, J.T., 2001. Oil and Shale Gas from the Barnett Shale, Fort Worth Basin, vol. 10. AAPG Annual Meeting Program, Texas, pp. A100.
Jenden, P.D., Kaplan, I.R., Poreda, R.J., Craig, H., 1988. Origin of nitrogen-rich natural gases in the California Great Valley: evidence from helium, carbon and nitrogen isotope ratios. Geochem. Cosmochim. Acta 52, 851–861.
Jenden, P.D., Titley, P.A., Worden, R.H., 2015. Enrichment of nitrogen and ^{13}C of methane in natural gases from the Khuff Formation, Saudi Arabia, caused by thermochemical sulfate reduction. Org. Geochem. 82, 54–68.
Jiao, W.W., Wang, S.X., Cheng, L.J., Luo, Q.Y., Fang, G.J., 2017. The reason of high nitrogen content and low hydrocarbon content of shale gas from the Lower Cambrian Niutitang Formation in southeast Chongqing. Nat. Gas Geosci. 28, 1882–1890 (in Chinese with English abstract).
Jurisch, A., Heim, S., Krooss, B.M., Littke, R., 2012. Systematics of pyrolytic gas (N_2, CH_4) liberation from sedimentary rocks: contribution of organic and inorganic rock constituents. Int. J. Coal Geol. 89, 95–107.
Jurisch, A., Krooss, B.N., 2008. A pyrolytic study of the speciation and isotopic composition of nitrogen in carboniferous shales of the North German Basin. Org. Geochem. 39, 924–928.
Kelemen, S.R., Gorbaty, M.L., Kwiatek, P.J., Fletcher, T.H., Watt, M., Solum, M.S., Pugmire, R.J., 1998. Nitrogen transformation in coal during pyrolysis. Energy Fuels 12, 159–173.
Kelemen, S.R., Afeworki, M., Gorbaty, M.L., Kwiatek, P.J., Sansone, M., Walters, C.C., Cohen, A.D., 2006. Thermal transformation of nitrogen and sulfur forms in peat related to coalification. Energy Fuels 20, 635–652.
Kotarba, M.J., Nagao, K., 2008. Composition and origin of natural gases accumulated in the Polish and Ukrainian parts of the Carpathian region: gaseous hydrocarbons, noble gases, carbon dioxide and nitrogen. Chem. Geol. 255, 426–438.
Kotarba, M.J., Nagao, K., Karnkowski, P., 2014. Origin of gaseous hydrocarbons, noble gases, carbon dioxide and nitrogen in Carboniferous and Permian strata of the distal part of the Polish Basin: geological and isotopic approach. Chem. Geol. 383, 164–179.
Krooss, B.M., Friberg, L., Gensterblum, Y., Hollenstein, J., Prinz, D., Littke, R., 2005. Investigation of the pyrolytic liberation of molecular nitrogen from Palaeozoic sedimentary rocks. Int. J. Earth Sci. 94, 1023–1038.
Krooss, B.M., Littke, R., Müller, B., Frielingsdorf, J., Schwochau, K., Idiz, E.F., 1995. Generation of nitrogen and methane from sedimentary organic matter: implications

on the dynamics of natural gas accumulations. Chem. Geol. 126, 291–318.
Kump, L.R., Arthur, M.A., 1999. Interpreting carbon-isotope excursions: carbonates and organic matter. Chem. Geol. 161, 181–198.
Lam, P., Lavik, G., Jensen, M.M., van de Vossenberg, J., Schmid, M., Woebken, D., Gutiérrez, D., Amann, R., Jetten, M.S.M., Kuypers, M.M.M., 2009. Revising the nitrogen cycle in the Peruvian oxygen minimum zone. Proc. Natl. Acad. Sci. Unit. States Am. 106, 4752–4757.
Lee, S.Y., Ryu, B.H., Han, G.Y., Lee, T.J., Yoon, K.J., 2008. Catalytic characteristics of specialty carbon blacks in decomposition of methane for hydrogen production. Carbon 46 (14), 1978–1986.
Leithold, E.L., Blair, N.E., Wegmann, K.W., 2016. Source-to-sink sedimentary systems and global carbon burial. Earth Sci. Rev. 153, 30–42.
Li, T., Tian, H., Xiao, X., Cheng, P., Zhou, Q., Wei, Q., 2017. Geochemical characterization and methane adsorption capacity of overmature organic-rich Lower Cambrian shales in northeast Guizhou region, Southwest China. Mar. Petrol. Geol. 86, 858–873.
Li, Z.Y., Elsworth, D., 2019. Controls of CO_2–N_2 gas flood ratios on enhanced shale gas recovery and ultimate CO_2 sequestration. J. Petrol. Sci. Eng. 179, 1037–1045.
Liang, C., Jiang, Z., Yang, Y., Wei, X., 2012. Shale lithofacies and reservoir space of the WufengeLongmaxi formation, Sichuan Basin, China. Petrol. Explor. Dev. 39, 736–743.
Littke, R., Krooss, B.M., Idiz, E., Frielingsdorf, J., 1995. Molecular nitrogen in natural gas accumulations: generation from sedimentary organic matter at high temperatures. AAPG Bull. 79 (3), 410–430.
Liu, Q.Y., Jin, Z.J., Chen, J.F., Krooss, B.M., Qin, S.F., 2012. Origin of nitrogen molecules in natural gas and implications for the high risk of N_2 exploration in Tarim Basin, NW China. J. Petrol. Sci. Eng. 81, 112–121.
Liu, H.M., Wei, G.L., Xu, Z., Liu, P., Li, Y., 2016. Quantitative analysis of Fe and Co in Co-substituted magnetite using XPS: the application of non-linear least squares fitting (NLLSF). Appl. Surf. Sci. 389, 438–446.
Liu, Y., Zhang, J., Ren, J., Liu, Z., Huang, H., Tang, X., 2016. Stable isotope geochemistry of the nitrogen-rich gas from lower Cambrian shale in the Yangtze Gorges area, South China. Mar. Petrol. Geol. 77, 693–702.
Luo, Q., George, S., Xu, Y.H., Zhong, N.N., 2016. Organic geochemical characteristics of the Mesoproterozoic Hongshuizhuang Formation from northern China: implications for thermal maturity and biological sources. Org. Geochem. 99, 23–37.
Maksimov, S.M., 1975. Origin of high-nitrogen gas pools. Int. Geol. Rev. 18 (5), 551–556.
Maloof, A.C., Ramezani, J., Bowring, S.A., Fike, D.A., Porter, S.M., Mazouad, M., 2010. Constraints on early Cambrian carbon cycling from the duration of the Nemakit-Daldynian-Tommotian boundary $\delta^{13}C$ shift, Morocco. Geology 38, 623–626.
Marty, B., Dauphas, N., 2003. Nitrogen isotopic compositions of the present mantle and the archean biosphere: reply to comment by pierre cartigny and magali ader. Earth Planet Sci. Lett. 216, 433–439.
Mastalerz, M., Drobniak, A., Stankiewicz, A.B., 2018. Origin, properties, and implications of solid bitumen in source-rock reservoirs: a review. Int. J. Coal Geol. 195, 14–36.
Mavridou, E., Antoniadis, P., Littke, R., Lücke, A., Krooss, B.M., 2008. Liberation of volatiles from Greek lignites during open system non-isothermal pyrolysis. Org. Geochem. 39, 977–984.
Mettam, C., Zerkle, A.L., Claire, M.W., Prave, A.R., Poulton, S.W., Junium, C.K., 2019. Anaerobic nitrogen cycling on a Neoarchaean ocean margin. Earth Planet Sci. Lett. 527. https://doi.org/10.1016/j.epsl.2019.115800.
Mingram, B., Hoth, P., Lüders, V., Harlov, D., 2005. The significance of fixed ammonium in Palaeozoic sediments for the generation of nitrogen-rich natural gases in the North German Basin. Int. J. Earth Sci. 94, 1010–1022.
Muradov, N.Z., Veziroglu, T.N., 2005. From hydrocarbon to hydrogencarbon to hydrogen economy. Int. J. Hydrogen Energy 30 (33), 225–237.
Nie, H., Zhang, J., Li, Y., 2011. Accumulation conditions of the lower cambrian shale gas in the Sichuan Basin and its periphery. Acta Pet. Sin. 32, 959–967 (in Chinese with English abstract).
Pan, C., Yu, L., Liu, J., Fu, J., 2006. Chemical and carbon isotopic fractionations of gaseous hydrocarbons during abiogenic oxidation. Earth Planet Sci. Lett. 246 (1–2), 70–89.
Pan, L., Xiao, X.M., Tian, H., Zhou, Q., Cheng, P., 2016. Geological models of gas in place of the Longmaxi shale in Southeast Chongqing, south China. Mar. Petrol. Geol. 73, 433–444.
Pels, J.R., Kapteijn, F., Moulijn, J.A., Zhu, Q., Thomas, K.M., 1995. Evolution of nitrogen functionalities in carbonaceous materials during pyrolysis. Carbon 33, 1641–1653.
Pecharsky, V.K., Zavalij, P.Y., 2003. Fundamentals of Powder Diffraction and Structural Characterization of Minerals. Kluwer Academic Publishers, New York, pp. 713.
Rodrı′guez-Reinoso, F., 1998. The role of carbon materials in heterogeneous catalysis. Carbon 36 (3), 159–175.
Stüeken, E.E., Kipp, M.A., Koehler, M.C., Buick, R., 2016. The evolution of Earth's biogeochemical nitrogen cycle. Earth Sci. Rev. 160, 220–239.
Stüeken, E.E., Zaloumis, J., Meixnerová, J., Buick, R., 2017. Differential metamorphic effects on nitrogen isotopes in kerogen extracts and bulk rocks. Geochem. Cosmochim. Acta 217, 80–94.
Su, Y., Wang, W., Li, J., Gong, D., Shu, F., 2019. Origin of nitrogen in marine shale gas in Southern China and its significance as an indicator. Oil Gas Geol. 40, 1185–1196 (in Chinese with English abstract).
Sweeney, J.J., Burnham, A.K., 1990. Evaluation of a simple model of vitrinite reflectance based on chemical kinetics. AAPG Bull. 74, 1559–1570.
Tan, J., Horsfield, b., Fink, R., Krooss, B., Schulz, H.-M., Rybacki, E., Zhang, J., Boreham, C.J., van Graas, G., Tocher, B.A., 2014. Shale gas potential of the major marine shale formations in the Upper Yangtze Platform, South China, Part III: mineralogical, lithofacial, petrophysical, and rock mechanical properties. Energy Fuels 28, 2322–2342.
Tan, J., Horsfield, B., Mahlstedt, N., Zhang, J., di Primio, R., Vu, T.A.T., Boreham, C., Graas, G., Tocher, B., 2013. Physical properties of petroleum formed during maturation of Lower Cambrian shale in the upper Yangtze Platform, South China, as inferred from Phase Kinetics modelling. Mar. Petrol. Geol. 48, 47–56.
Tian, H., Pan, L., Xiao, X.M., Wilkins, R.W.T., Meng, Z.P., Huang, B.J., 2013. A preliminary study on the pore characterization of Lower Silurian black shales in the Chuandong Thrust Fold Belt, Southwestern China using low pressure N_2 adsorption and FE-SEM methods. Mar. Petrol. Geol. 48, 8–19.
Tian, H., Pan, L., Zhang, T.W., Xiao, X.M., Meng, Z.P., Huang, B.J., 2015. Pore characterization of organic-rich lower cambrian shales in qiannan depression of Guizhou province, southwestern China. Mar. Petrol. Geol. 62, 28–43.
Wang, D., Ling, H.F., Struck, U., Zhu, X.K., Zhu, M., He, T., 2018. Coupling of ocean redox and animal evolution during the Ediacaran-Cambrian transition. Nat. Commun. 9 (1), 1–8 2575.
Wang, D., Struck, U., Ling, H.F., Guo, Q.J., Shields Zhou, G.A., Zhu, M.Y., Yao, S.P., 2015. Marine redox variations and nitrogen cycle of the early Cambrian southern margin of the Yangtze platform, South China: evidence from nitrogen and organic carbon isotopes. Precambrian Res. 267, 209–226.
Waples, D.W., 1980. Time and temperature in petroleum formation: application of Lopatin's method to petroleum exploration. AAPG Bull. 64, 916–926.
Wu, Y., Gong, D., Li, T., Wang, X., Tian, H., 2019. Distribution characteristics of nitrogen-bearing shale gas and prospective areas for exploration in the Niutitang Formation in the Qianzhong uplift and adjacent areas. Geochimica 48, 613–623 (in Chinese with English abstract).
Yin, L., Li, J., Tian, H., Long, X.P., 2018. Rhenium–osmium and molybdenum isotope systematics of black shales from the Lower Cambrian Niutitang Formation, SW China: evidence of a well oxygenated ocean at ca. 520 Ma. Chem. Geol. 499, 26–42.
Zeng, X.L., Liu, S.G., Huang, W.M., Zhang, C.J., 2012. Comparison of silurian Longmaxi Formation shale of Sichuan Basin in China and carboniferous barnett formation shale of fort worth basin in United States. Geol. Bull. China 30, 372–384 (in Chinese with English abstract).
Zhang, M.J., Tang, Q.Y., Cao, C.H., Lv, Z.G., Zhang, T.W., Zhang, D.K., Li, Z.P., Du, L., 2018. Molecular and carbon isotopic variation in 3.5 years shale gas production from Longmaxi Formation in Sichuan Basin, China. Mar. Pet. Geol. 89, 27–37.
Zhang, S., Zhang, B., Bian, L., Jin, Z., Wang, D., Chen, J., 2007. The Xiamaling oil shale generated through Rhodophyta over 800 Ma ago. Science in China Series D: Earth Sci. 50, 527–535.
Zhang, Y., Chi, Y., Xing, W.L., Liu, S.Y., Song, Y.C., 2017. Competitive adsorption/desorption of $CH_4/CO_2/N_2$ mixture on anthracite from China for ECBM operation. Energy Procedia 105, 4289–4294.
Zhu, Y., Shi, B., Fang, C., 2000. The isotopic compositions of molecular nitrogen: implications on their origins in natural gas accumulations. Chem. Geol. 164, 321–330.
Zou, C., Dong, D., Wang, S., Li, J., Li, X., Wang, Y., Li, D., Cheng, K., 2010. Geological characteristics and resource potential of shale gas in China. Petrol. Explor. Dev. 37, 641–653.
Zou, C.N., Dong, D.Z., Wang, Y.M., Li, X.J., Huang, J.L., Wang, S.F., Guan, Q.Z., Zhang, C.C., Wang, H.Y., Liu, H.L., Bai, W.H., Liu, D.X., Yang, Z., Liang, P.P., Sun, S.S., Qiu, Z., 2015. Shale gas in China: characteristics, challenges and prospects (II). Petrol. Explor. Dev. 43, 753–767.